Activation and suppression of NF-κB signaling via miRNA in a chemoresistant cancer model

Sonja Maria Katz

University of Natural Resources and Life Sciences, Vienna

Supervisor

ao. Univ.Prof. Dr. Robert Mader

In partial fulfillment of the requirements for the degree of

Master of Science in Biotechnology

Vienna, October 2019

Erklärung der Urheberschaft

Ich erkläre hiermit an Eides statt, dass ich die vorliegende Arbeit ohne Hilfe Dritter und ohne Benutzung anderer als der angegebenen Hilfsmittel angefertigt habe; die aus fremden Quellen direkt oder indirekt übernommenen Gedanken sind als solche kenntlich gemacht. Die Arbeit wurde bisher in gleicher oder ähnlicher Form in keiner anderen Prüfungsbehörde vorgelegt und auch noch nicht veröffentlicht.

Wien, 3.10.2019 Sonja Maria Katz

Contents

List of Figures

List of Tables

Abstract

Treatment of colonic cancer with an acquired resistance to chemotherapeutic agents such as 5-fluorouracil (5-FU) has been posing a major challenge in modern medicine. In recent years, small non-coding RNAs termed microRNAs (miRNAs) were found to act as potent post-transcriptional regulators and their aberrant expression linked to various malignancies. Involvement of miRNAs in sustaining a proinflammatory response *via* activation of the NF-κB signaling pathway has proven to be crucial for tumor progression, as well as development of resistance against 5-FU. In this study, we aim to unravel modulation of NF-κB signaling by miRNAs differentially expressed in colon carcinoma cell lines non-sensitive and highly sensitive to 5-FU.

Our multi-stage resistant colonic carcinoma model comprised a primary adenocarcinoma (CCL228), its lymph node metastasis (CCL227), and three resistant subclones with progressing stages of resistance against 5-FU. miRNAs differentially expressed in 5-FU sensitive
(CCL228, CCL227) and completely insensitive (high resistance phenotype) cell lines were determined by conducting microRNA array analysis. Impact of a selection of non-coding RNA on the NF-κB signaling pathway were evaluated using a luminescent assay as well as quantitative real-time PCR measurements. Whether post-transcriptional gene regulation by RNA interference is sufficient to alter the response of resistant cell lines to 5-FU was determined by cytotoxicity assays.

Our data revealed, that direct targeting of the p65 subunit with p65-siR is a highly potent way to abrogate NF-κB activation. Reduction in protein levels of up to 65% compared to the native state was observed. Viability assays showed, that introduction of p65-siR results in diminished tolerance to 5-FU. The set of deregulated miRNAs selected for further analysis included miR-141, a suspected NF-κB suppressor, as well as miR-375 and miR-125b, which are assumed to possess pro-inflammatory properties by activating NF-κB signaling. Whilst miR-141 exhibited suppression of NF-κB, the observed efficiencies were minor. Although miR-375 was identified as potential stimulator by our miRNA array, it displayed consistent suppressing properties. For miR-125b, no distinct modulations could be observed.

In summary, we found small regulatory sequences to be able to efficiently modulate NF-κB levels *in vitro* and even suspect them to be capable of restoring susceptibility of resistant phenotypes to 5-FU. However, careful selection of introduced RNA is a premise, for our data showed that transfection of single miRNAs alone can not be regarded as reliable and efficient regulatory mechanism. This also implies, that deregulated miRNAs should not be analysed individually when aiming to explain complex phenotypic behavior.

Introduction

1.1 Colorectal cancer

Cancer is a malignant disease which has developed to one of the greatest challenges modern medicine has ever faced. According to the International Agency for Research on Cancer, around 9.5 million cancer deaths occurred in 2018 alone, with additionally 18 million new cases being recorded. The third most abundant cancer type is colorectal cancer (CRC), accounting to 10.2% of all incident cases worldwide. Treatment of CRC initially based on 5-fluorouracil (5-FU), a fluorinated pyrimidine acting as uracil analogue and interfering in nucleoside metabolism, thus leading to cytotoxicity and cell death [1, 2]. Administration of intravenous fluorouracil doubled the median survival among patients with metastatic colorectal cancer from an average of 6 months to 12 months. Actual combination therapies additionally include another active cytotoxic chemotherapeutic agent such as oxaliplatin or irinotecan, further prolonging patient lives [1, 3]. The efficacy of fluorouracil-based chemotherapy has been firmly established, but clinical applications have been greatly limited due to drug resistance [4]. Nevertheless, 5-FU remains a cornerstone in current systemic combination therapies, therefore circumvention of resistance is of profound importance.

1.2 Resistance to 5-FU in colorectal cancer cells

Current oncological research often focuses on molecular mechanisms causing resistance in order to further understand cancer dynamics and circumvent respective defenses, ensuring a longer therapeutic success and inherent patient survival rates. Resistance mechanisms against 5-FU include alterations of drug influx and efflux, increased expression and mutation of the drug target, as well as increased catabolism of fluorouracil through overexpression of degrading enzymes [2, 5]. In-depth analysis of genomic alterations conferring resistance were conducted using expression profiling of cellular RNA. Recent studies have proven that acquisition of resistances is a highly complex process which can not be determined by a few key proteins, but involves more than 300 genes. Furthermore, the dependency on time is an important aspect when describing drug resistance. Very commonly, different stages of resistance can be observed, each characterized by unique alterations in expression patterns. Especially in early stages cells are challenged to adopt to the new conditions, which is reflected by heavy alterations in protein levels. In contrast, the transition to a high-resistance phenotype affects significantly less genes [6].

Initial resistance acquirement is known to be promoted by inflammatory cell responses, especially in inflammation-associated cancers such as CRC [7]. It was shown, that the tumor microenvironment is governed by inflammatory cells actively secreting mediator molecules such as tumor necrosis factor-α (TNF-α), cytokines, growth factors and cytokines [8]. These signaling molecules are able to induce specific cell responses by binding to cell-surface receptors, thereby triggering signaling cascades ultimately activating transcription factors, which alter gene expression [9]. In particular TNF-α and IL-1 cytokines are major inducers for nuclear factor kappa B (NF-κB), a transcription factor family essential for inflammation, cell proliferation and apoptosis [10, 11]. Cancer cells displaying a resistant phenotype to chemother-

apeutic agents have shown to constitutively activate NF-κB, whereas their mother cell line displayed no activation at all [12]. Going in accordance with this, numerous studies have linked elevated NF-κB levels to tumor progression and poor diagnostic outcomes [13, 14, 15, 16]. Vice versa it has been shown, that compounds able to block NF-κB activation are able of abrogating malignant cell growth [17, 18]. Working with a CRC *in vitro* model exhibiting different stages of resistance to 5-FU showed that inhibition of essential steps in the NF-κB signaling pathway can even lead to restoration of sensitivity to the chemotherapeutic agent [12]. The benefits of lowering malignant NF-κB levels seem to be manifold, which sparked the interest in developing new methods to efficiently counter NF-κB overexpression.

1.3 The NF-κB signaling pathway

The NF-κB family is composed of five member proteins: Rel (c-Rel), RelA (p65), RelB, NFκB1 (p50) and NFκB2 (p52). These proteins form heterodimeric complexes which are abundant in the cell cytoplasm of every cell but reside in a latent state. This idle mode is mediated through interaction with inhibitory proteins belonging to the IκB protein family. Abrogation of the latent state requires activation of NF-κB through an activational signaling cascade. The two evolutionary most conserved pathways known to stimulate NF-κB are the so-called canonical and the non-canonical pathways. The first one, also known as classical pathway, is induced through external stimuli such as TNF-α, IL-1, or genotoxic agents. Upon stimulation, IκB molecules are phosphorylated by the IκB kinase complex (IKK), which results in their proteasomal degradation. The now free RelA:p50 dimers are able to translocate into the nucleus, where they bind target gene sequences and enhance their transcription. The non-canonical pathway is activated by a more restricted set of signaling molecules, but works similar to its classical equivalent. It is initiated by

the NF-κB-inducing kinase (NIK) which activates IKK, leading to the degradation of the RelB inhibitor p100. Subsequently, formation of RelB:p52 complexes are able to alter gene expression [19]. When speaking about NF-κB as transcription factor, mostly the complexes RelA:p50 or RelB:p52 are referred to, due to them being the active part capable of translocating into the nucleus. Both pathways thus rely on sequentially activated kinases phosphorylating NF-κB inhibitory molecules. For the canonical pathway, this has been demonstrated by the inability of mutants which can not phosphorylate IκB, to activate NF-κB [20]. Another mechanism required for optimal induction of NF-κB target genes requires phosphorylation of NF-κB subunits, for expample of p65. Phospho-p65 has been shown to enable optimal binding of the NF-κB complex to DNA [21].

The complexity and sequential stages of the NF-κB signaling cascade enables numerous regulatory mechanisms to tightly control NF-κB activation. A total of 154 positive and 88 negative modulators of NF-κB signaling have been described so far. This allows for layers of control within the system, making this pathway remarkably robust [22]. Nevertheless, several key regulatory systems have been identified, leading to the development of inhibitory agents abrogating NF-κB activation. Some of these will be discussed below.

1.3.1 IκBα super-repressors

Inspired by the inability of IκBα mutants to activate NF-κB led to therapeutic approaches using non-degradable IκB protein, so called IκBα super-repressors. This variant of the NF-κB inhibtory protein IκB shows mutations in two serine residues, preventing phosphorylation by IKKα. Subsequently, the protein can not get degraded by the proteasome, which sustains its inhibitory potential. The adenoviral delivery of IκBα super-repressors to chemoresistant tumors in mice, sensitizes the cells to undergo apoptosis under treatment with TNF-α, leading to tumor regression

[23].

1.3.2 IKK inhibitors

Instead of directly stabilizing the NF-κB inhibitor as in the case of IκBα super-repressors, also the kinase marking IκB as degradable target can be inhibited. Therapeutic agents targeting the catalytic subunit of IKK (IKKβ) have been shown to cause apoptosis of cancer cells *in vitro* and *in vivo*. Compounds of such kind mostly act as competitive inhibitors of the active site, inhibiting subsequent IκBα phosphorylation [24, 25].

1.3.3 Proteasome inhibitors

It is currently well understood that the proteasome pathway plays a critical role in the formation and activation of different NF-κB complexes. One of the first approved drugs for treatment of multiple myeloma, a disease heavily dependent on NF-κB activation, was the proteasome inhibitor bortezomib [26]. Although bortezomib lacked clinical evidence in the treatment of solid tumors, similar compounds have displayed growth arrest and apoptosis of glioblastoma multiforme in preclinical models [27]. In recent years, a number of different drugs targeting the proteasome pathway have emerged and extensively studied, exhibiting promising results in terms of efficacy. Comparing direct targeting of the proteasome to approaches modulating precursors upstream, such as IKKβ or IκB, renders inhibition of the proteasome activity significantly more potent [28].

Although all classes of agents described above have been proven efficient down-regulators of the RelA:p50 complex, drug specificity is an unmatched problem. The integrity of the proteasome, for example, is vital to normal cell function in any tissue. Drugs targeting this pathway often show numerous side effects, such as gastrointesti-

nal symptoms, anemia, thrombocytopenia, fatigue, and peripheral neuropathy in the case of bortezomib [29]. Additionally, inhibiting NF-κB for a prolonged period of time might be not be feasible due to its importance in maintenance of host cell defense. This is corroborated by the observation, that mutant mice expressing the IκBα super-repressors are more prone to suffer from bacterial infections [30].

The potential of NF-κB as therapeutic target has been intensely studied, giving rise to a broad number of agents modulating different key players in the signaling chain. However, few of these substances proceed to a clinical setting, due to frequently observed unspecificity and toxicity.
Over the past years, microRNA have risen to popularity due to their potent gene regulating abilities. They have proven to be highly specific, dramatically reducing unwanted off-target toxicities. Therefore, they have gained attention as potential novel therapeutic agent, also in the context of NF-κB modulation.

1.4 microRNA

MicroRNAs (miRNAs, miRs) are a subfamily of non-coding regulatory RNA with a size of 18-22 nt, involved in post-transcriptional silencing of genes. They are initially transcribed by RNA polyermase II or RNA polyermase III, as a long primary transcript (pri-miRNA). This transcript is further cleaved in the nucleus by the Drosha-DGCR8 complex and exported to the cytoplasm in form of the hairpin-shaped pre-miRNA. The last cleaving step by the endoribonuclease protein called Dicer produces miRNA of appropriate length. The mature miRNA is incorporated in the RNA-induced silencing complex (RISC), formed by members of the argonaute protein family. In this complex it acts as specificity conferring element, due to its ability to bind to partially complementary sites in the 3' untranslated region (3'

UTR) of messenger RNA (mRNA). Binding to target mRNA results in impairment of further translation by inhibiting translation initiation, as well as decreasing mRNA levels through cleavage [31, 32, 33]. During the past decade, they have received increasing attention due to their ability to selectively target and inhibit mRNA transcripts and therefore alter gene expression post-transcriptionally [34].

1.4.1 microRNAs in cancer

Today, miRNAs are known to play an important role in regulation of all biological pathways, functioning in feedback mechanisms to maintain normal cellular responses to extracellular stimuli. This has led to emerging evidence of the pivotal role miRNA play in malignancies, particularly cancer. De-regulation of a small subset of miRNAs can affect expression patterns of several hundred mRNAs, promoting cellular instability [32, 35]. Sequencing data obtained from a variety of cancer tissue samples has confirmed, that abnormal miRNA expression is highly abundant and suspected to be essential for cancer progression [36].

The underlying mechanisms leading to dysregulation of miRNA in malignancies are of diverse nature. A frequently observed cause are genomic alterations, mainly amplification, deletion or translocation of genes coding for miRNAs. Genes located in regions that are amplified in cancer frequently function as oncogenes, whereas domains deleted confer tumor suppressing functions. Furthermore, miRNA expression is tightly regulated by transcription factors such as c-Myc and p53. It has been shown, that the tumor suppressor p53 performs its apoptotic function through directly binding to promotor regions of several miRNAs involved in the apoptotic cell response. p53 is one of the most commonly mutated genes in human cancer, hinting at the impact transcription factor dysregulation can have on miRNA expression. Also miRNA biogenesis is a complex task involving several key enzymes. Modulation of any processing enzyme might lead to unnatural miRNA levels, resulting in

a malignant phenotype [37, 38].

It is currently well established, that this subfamily of non-coding regulatory RNA can function as either oncogene or tumor suppressor, depending on the circumstances. To further describe their impact on tumor formation, their functions can be analyzed with respect to the hallmarks of cancer. These hallmarks, as proposed by Hanahan and Weinberg, aim to rationalize the complexity of cancer progression by classifying six biological capabilities acquired during development of neoplasms [39]. miRNA have been shown to be involved in several of them, including sustaining of proliferative signaling, evading growth suppressors, resisting cell death, inducing angiogenesis, and activating invasion and metastasis [37]. Irrespective of their function, analysis of miRNA expression profiles provides a fingerprint, allowing for classification of different tumor characteristics, such as tissue type, aggression and response to therapy. This raises the hope, that miRNA circulating in the blood stream provide a potential source of biomarkers and profiling techniques can be utilized for patient prognosis and prediction of clinical response [35, 40].

The nature of miRNA allowing for regulation of several target genes, poses a challenge when aiming to uncover their complex roles in malignancies. Although much effort has been put into studying miRNAs, our knowledge of their full potential is still limited. However, their importance as regulatory elements and their impact on cancer formation has led to novel treatment approaches focusing on dysregulated miRNA, with the aim to restore their native functions. Overexpressed oncogenic miRNAs are targeted by small-interfering RNA (siRNA), selectively lowering malignant levels. These siRNA transcripts are commonly termed anti-miRs. Lost tumor-suppressor functions can be reintroduced by transfecting synthetic miRNA, so-called miR-mimetics [41]. With the first patent for applications using miRNA being granted in 2008, the number of filed patents has exploded over the last decade to a total of more than 2000 in the year 2017. Development of miRNA-

targeted therapeutics is ongoing, with several anti-miR or miR-mimetics having already reached clinical trials, also in the form of combinational approaches using conventional chemotherapy agents. Limitations and drawbacks of this novel treatments are accurate delivery of the RNA sequences to target cells, dose-dependent toxicity, and biosafety [42, 43]. Regardless, RNA-based therapeutics will potentially overcome these obstacles, entering clinical settings as next generation drug with the ability to contribute to the future of medicine.

1.4.2 microRNA and the NF-κB signaling pathway

The physiological roles of miRNA include regulation of cell proliferation, inflammation and apoptosis, functions also known to be controlled by NF-κB. This has led to various studies identifying miRNA targets in the NF-κB signaling cascade, as well as linking them to cancer formation and progression [44]. In this section, connections between miRNA and the NF-κB signaling pathway will be discussed.

Very commonly, miRNA do not target the transcription factor complex itself, but proteins upstream in the signaling cascade. They have been shown to already be involved in the regulation of tumor necrosis factor receptor-associated factor (TRAF), a key protein in cellular signal transduction upon receptor binding. By targeting TRAF6, miR-146 is able to suppress subsequent NF-κB activation [45]. Another potent way of modulating NF-κB is by directly targeting IκBα. In prostate cancer cells, NF-κB is chronically activated by hyper-expression of miR-30e*. This miRNA drives cancer cell proliferation and tumor growth through suppression of IκB, resulting in elevated levels of free NF-κB ready to translocate into the nucleus [46]. An example of a positive feedback loop activating NF-κB by indirectly acting on IκB is miR-125b. It represses TNF-induced protein 3 (TNFAIP3), an enzyme possessing deubiquitinase activity which actively removes degradation tags from IκB, therefore limiting NF-κB activation upon bacterial infections [47].

But not only do miRNA interfere in the NF-κB signaling pathway, also the vice versa regulation of miRNA levels by the transcription factor is possible. Genes coding for miRNA possess NF-κB binding sites in the promotor region, enabling enhanced transcription rates upon pro-inflammatory stimuli. This mechanism indirectly links NF-κB activity to other cellular pathways, which are primarily regulated by miRNA [48].

Recently, a growing number of reports confirm that aberrant expression of miRNA targeting parts of the NF-κB signaling cascade can be linked to cancer phenotypes showing resistance to various chemotherapeutic treatments. The causes for multidrug resistance (MDR), as mostly acquired after an initial round of treatment, are diverse and not yet fully understood. However, differentially expressed miRNA involved in regulation of genes crucial for the resistant phenotype, are frequently observed to be dysregulated [49]. Supporting this theory, miRNA have been demonstrated to be able to even resensitizes resistant cell lines to chemotherapeutic agents. Using a colon carcinoma model with acquired resistance to 5-FU, Zhao and coworkers have demonstrated miR-15b-5p overexpression to promote apoptosis and reverse chemoresistance. miR-15b-5p is a key tumor suppressor miRNA, which is globally decreases in CRC tissue. It acts by promoting apoptosis through negatively regulating IKK-α, thus preventing IκB phosphorylation and subsequent NF-κB activation [50].

This study, amongst many others, raise the hope that targeting miRNA responsible for deregulation of the NF-κB pathway is a promising strategy for the treatment of malignant diseases. Several miRNA antagonists (anti-miR) have demonstrated a strong potential to downregulate endogenous miRNA targets [51]. In a lung carcinoma model, inhibition of the overexpressed miR-223 by anti-miR-223 resulted in significantly reduced cell viability and invasiveness. Detailed analysis of the underlying mechanism revealed a decrease in expression levels of phosphorylated NF-κB

(p-NF-κB), as well as p-IKKα/β and p-IκB. Addition of a synthetic NF-κB inhibitor further enhanced the inhibitory effects of anti-miR-223 on cell invasion [52]. Upregulated miR-21 expression has been identified as crucial for colon carcinoma formation and progression. Transient transfection of antisense oligonucleotides against miR-21 efficiently decreased relative expression of miR-21 in an *in vitro* colon model, accompanied by impaired cell proliferation, clone formation, invasion and migration [53, 54]. Not only targeted degradation of selective oncogenic miRNAs can have a favorable therapeutic effect, also synthetic miRNAs can be applied to restore loss of function in malignant tissue, so-called miRNA mimetics [36]. Introduction of miRNA mimetics was shown to be able to increase target protein expression to up to 50%. An example of their potency are miR-141 mimetics, which are able to enhance resistance to cisplatin in an ovarian carcinoma model while also activating the NF-κB signaling pathway [55, 56].

Up to today, therapeutics focusing on miRNAs were able to selectively target parts of the NF-κB signaling cascade and have antagonistic effects on cancer progression and tumor formation. Especially their potential to resensitize cells with acquired resistances to common chemotherapeutic agents, makes them a valuable supplement to conventional treatments. Combinational therapies of such kind have already entered preclinical stages and could redefine state-of-the-art treatments [57].

1.5 Aims of this thesis

Summarizing above mentioned literature, miRNAs have been demonstrated to be involved in formation and progression of various types of cancer, also through regulation of the NF-κB signaling pathway. NF-κB activation has been identified as tumor promoting factor, as well as major player in cellular resistance mechanisms against chemotherapeutics.
The aim of this study was to investigate the impact of several selected miRNAs on NF-κB regulation. A number of miRNAs are differentially expressed in a colon carcinoma model with differing stages of resistance against the chemotherapeutic agent 5-FU. We hypothesized, that miRNA highly abundant in cells being unresponsive to 5-FU have tumor promoting functions, whereas miRNA present in chemotherapy-sensitive cell lines could pose as potential tumor suppressors.

Following research questions have been formulated:

- Do miRNA overexpressed in a cell line highly resistant to 5-FU stimulate NF-κB expression in naïve colon carcinoma cells?
- Can miRNA overexpressed in cell lines sensitive to 5-FU lower malignant NF-κB levels in resistant cells?
  - If yes, are introduction of these miRNA-mimetic sufficient to reverse chemoresistance?

Methodology

2.1 Culturing cells

For assessing the impact of specific miRNA on the NF-κB signaling pathway in a cancer model showing resistance to 5-FU, a multi-stage resistant colonic carcinoma model system was used. It comprised the mother cell lines CCL228 (also known as SW480), which is a primary adenocarcinoma, and its lymph node metastasis CCL227 (SW620). Both cell lines were obtained from the American Type Culture Collection (ATCC). Additionally, three subclones with an increasing resistance to the chemotherapeutic agent 5-fluorouracil (5-FU) were produced from cell line CCL227 (see table 2.1). From these, resistant subclones with identical generation time have been selected to eliminate cell cycle effects from the cellular models.

Table 2.1: Concentration of 5-FU in cell culture medium.

Cell line	Resistance against 5-FU
CCL228	0 μM
CCL227	0 μM
CCL227 + 5 μM 5-FU (low resistance)	5 μM
CCL227 + 25 μM 5-FU (intermediate resistance)	25 μM
CCL227 + 125 μM 5-FU (high resistance)	125 μM

All cell lines were cultivated in T75 flasks with RPMI 1640 media supplemented with Glutamax-I (Gibco) and 10% exosome-free fetal calf serum (FCS) (Sigma) at

37 °C in a humidified atmosphere of 5% CO_2 and 95% air. Exosome-free FCS was obtained by sequential high-speed and ultracentrifugation steps, followed by sterile filtration. To ensure cell viability and avoid overgrowth, cell lines were passaged two times a week in sterile environment, when cell confluency had reached approximately 80%. Therefore, supernatant media was discarded and cells washed with equivalent volume of 1x DPBS (Gibco) before being detached with 1x Accutase (Sigma). Cells were resuspended in RPMI 1640 + 10% FCS (exosome-free) and centrifuged at 287xg for 5 minutes. The pellet was dissolved in media and a specific volume transferred back into the cultivation flask, depending on the growth rate of corresponding cell line. By addition of media the final cultivation volume of 10 mL was reached. The resistant subclones were further supplemented with 5-FU from a 60 nM stock solution (5-FU dissolved in 0.9% NaCl) in order to ensure a final concentration of 5 μM, 25 μM or 125 μM in the cultivation media.

2.2 Assessment of NF-κB levels using a reporter system

2.2.1 Cignal Reporter Assay

In order to monitor changes in the expression of genetic elements, firefly luciferase assays have proven to be reliable, sensitive and easy to use systems. Therefore, the QIAGEN Cignal Report Assay has been chosen to assess up- and downregulation of the transcriptional factor NF-κB. This assay consists of combinations of two different luciferases and GFP under the control of variously active promotors or enhancing elements. This ensures reproducible and interpretable results. Below, each combination is depicted and its purpose explained.

2.2.1.1 Positive control

The Cignal Positive Control (abbreviated as Cignal Positive or positive Cignal) encodes the Firefly and *Renilla* luciferase, as well as Monster-GFP, all under the control of a constitutively active CMV promotor (figure 2.1). The positive control helps optimizing the transfection conditions and provides a visual control of transfection efficiency through GFP. Hence it was included in every experiment. Each of the three elements are present as individual construct and transfected as a mixture, with a ratio of 40:1:1 (firefly : *Renilla* : GFP).

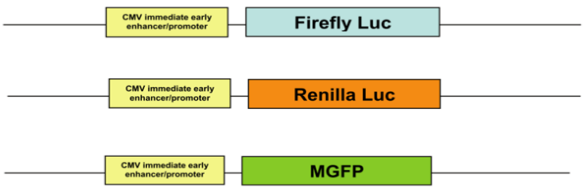

Figure 2.1: Cignal Dual Luciferase System - elements included in positive control

2.2.1.2 Reporter construct

The transfection mix simply abbreviated as ,,Cignal" are the reporter constructs used to measure NF-κB activity (ratio firefly : *Renilla* = 40 : 1). Besides an inducible promotor element featuring four NF-κB binding sites controlling the expression of Firefly luciferase, *Renilla* is expressed constitutively (figure 2.2). This allows for normalization of the firefly signals in respect to *Renilla*, compensating differences in transfection efficiencies. Normalization is performed by calculating the ratio of firefly signal to *Renilla* signal for each replica (2.1).

$$\text{ratio} = \frac{Signal(firefly)\ [LU]}{Signal(Renilla)\ [LU]} \tag{2.1}$$

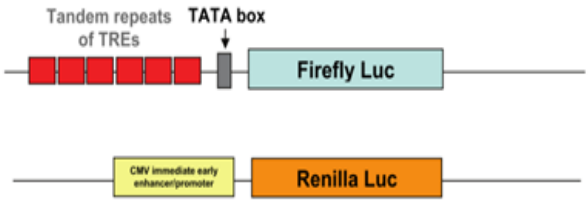

Figure 2.2: Cignal Dual Luciferase System - elements included in reporter

2.2.1.3 Negative control

,,Negative Cignal" is the negative control provided in the reporter kit and contains the firefly luciferase without a control element (only TATA box) and *Renilla* under a CMV promotor (ratio 40 : 1) (figure 2.3). It is mainly used to determine background reporter activities and quantify unspecific effects that may occur.

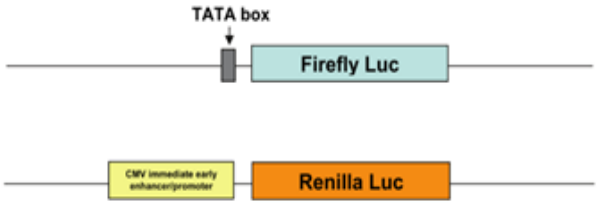

Figure 2.3: Cignal Dual Luciferase System - elements included in negative control

2.2.2 Optimization of transfection conditions

The sensitivity of reporter systems can be greatly increased by high transfection efficiencies. Optimal transfection conditions are very cell line specific, therefore the default transfection protocol suggested by the manufacturer was modified accordingly. Parameters such as cell count and incubation time were varied in preliminary experiments to maximize transfection success.

2.2.2.1 Determination of the optimal cell count

Cell line CCL227 was seeded in a fresh flask and grown to 70% confluency. The cell suspension obtained after detaching of cells was centrifuged and resuspended in fresh RPMI media (0% FCS). Cell densities were estimated by counting the cells using a Brker-Trk counting chamber and diluted in order to obtain the final well concentrations depicted in table 2.2.

Table 2.2: Summary of cell counts used to optimize transfection

number of cells per well [cells/well]
1 x 10^4
2 x 10^4
4 x 10^4
6 x 10^4
8 x 10^4
10 x 10^4

Without variation in procedure, volume of transfection reagent or volume of plasmid solution (for more detail see section 2.2.3), these six different cell counts were evaluated. As seen in figure 2.4, signals deriving from the firefly luciferase (green line) and *Renilla* luciferase (purple line) correlate very well, eliminating the fear of potential unspecific interactions, especially when using higher cell concentrations. Cell counts below 4 x 10^4 do not result in a sufficiently high luciferase signal. Numbers higher than 8 x 10^4 show a decline in luminescent signal, indicating a lack of either transfection reagent or plasmid solution. Taking into account the original protocol by QIAGEN and visual analysis of cell densities, a cell count of 4 x 10^4 cells per well was chosen for further experiments.

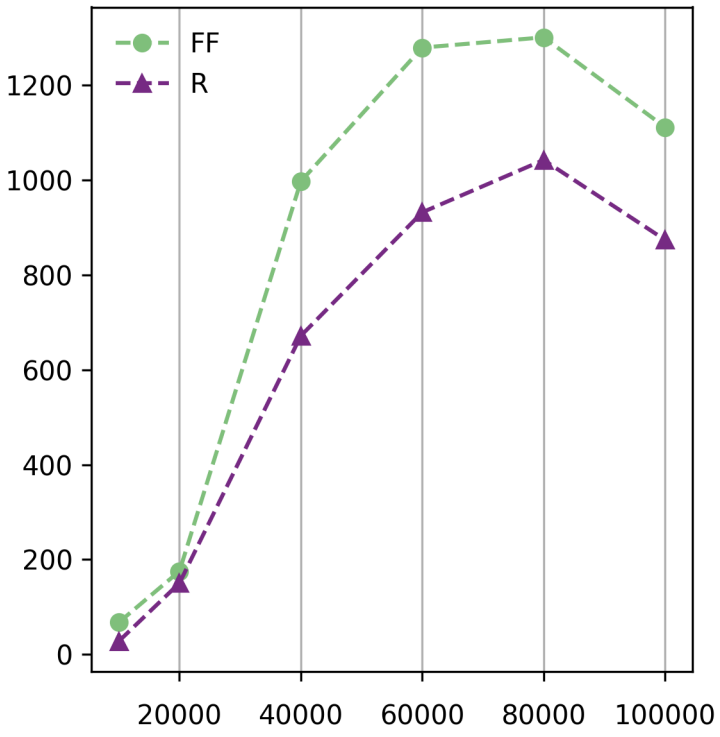

Figure 2.4: Assessment luminescent signal using various cell counts in CCL227. The green dashed line corresponds to the firefly signal (FF), whereas the purple dashed line derives from *Renilla* signals (R).

2.2.2.2 Variation of incubation time

Following reverse transfection of cells, the manufacturer suggests an incubation period of 24-48 hours at 37°C in a humidified atmosphere of 5% CO_2 and 95% air. Subsequently, measurement of luminescent signals can be conducted. To investigate the influence of varying incubation times on signal intensities, the high resistance cell line was transfected with reporter and negative siR (for more details see section 2.2.3) were divided into three plates and incubated for 24 hours, 48 hours and 72 hours. Figure 2.5 shows, that maximum intensities for each luciferase (green: firefly luciferase, purple: *Renilla* luciferase), as well as their calculated ratio (grey dashed), were obtained upon incubation for 24 hours.

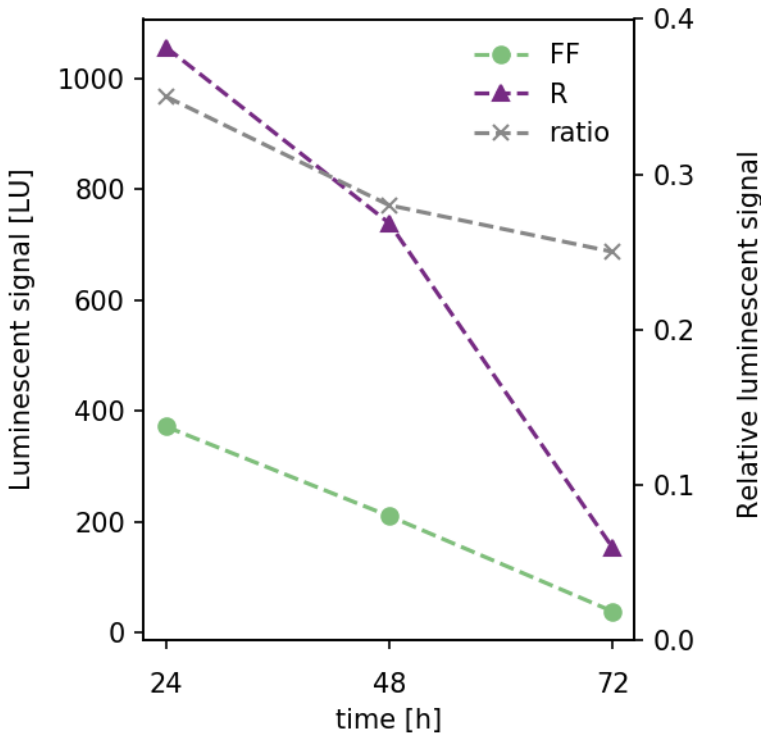

Figure 2.5: Dependency of luminescent signal on incubation time in cell line CCL227. Three different time spans were assessed, including 24 hours incubation time, 48 hours and 72 hours. The green line corresponds to the raw firefly signal, purple to the *Renilla* luciferase and the grey line is the calculated ratio firefly/*Renilla*.

Time spans exceeding the 24 hour mark show a steady decrease in signal. Additionally notable here is the rather minor change in the ratio when compared to the raw signals, as seen around 72 hours. Although signals of both luciferases drop significantly, the ratio does not resemble this. This hints at the robustness of evaluating the ratio of two signals rather than their individual intensities. In summary, this preliminary experiment suggests an incubation time of 24 hours prior to measurement.

2.2.2.3 NF-κB induction using IL-1α

Recombinant interleukin-1 (IL-1) α and β are known to be potent activators of cytosolic NF-κB and can therefore directly be linked to be a mediator of inflammatory reactions [58]. Previous work has shown, that stimulation in rat glioma cells using IL-1 in the micromolar range induces a significant raise in NF-κB expression after only 20 minutes, lasting up to 24 hours [59]. In an attempt to increase NF-κB baseline activities in CRC cells, they were stimulated for 4 hours using different concentrations of IL-1α (purchased from Thermo Fisher; cat. no. 50114MNAE25). For further details and results please see section 3.3.

2.2.3 Transfection of Cignal Dual-Luciferase Reporter Assay and siRNA/miRNA

Cells were transfected using a transfection mixture consisting of Cignal reporter plasmid (QIAGEN), specific RNA (QIAGEN, AMBION) and Attractene transfection reagent (QIAGEN), all diluted in serum-free RPMI Medium 1640 supplemented with GlutaMAX^{TM} (Gibco).

Table 2.3 displays the per well components needed for each transfection without extra amount compensating for pippeting errors. For the nucleic acid mix, 11.4 μL of RPMI media (0% FCS) was added to a polystyrene tube, along with 100 ng

(= 1 μL) of reporter plasmid (Cignal positive control, Cignal reporter or Cignal negative control), as well as 2 pmol (= 0.1 μL of a 20 μM stock solution) of RNA (sequence-specific miRNA/siRNA or negative control siRNA). The final nucleic acid mix should have a total volume of 12.5 μL. The Attractene mix was prepared by dispersing 0.6 μL of well mixed Attractene transfection reagent in 11.9 μL of RPMI media (0% FCS). After mixing gently by pipetting an incubation time of 5 minutes was started. Subsequently, 12.5 μL of Attractene mix was added to each of the tubes containing 12.5 μL diltued nucleic acids, which results in an equal amount of transfection reagent and nucleic acids (1:1 ratio). Mixing must be done very gently in order not to impede complex formation. Therefore, gentle tapping against the tube while combining, as well as very slow up and down pippeting is advised. To allow complex formation to occur, the mixture is incubated for 20 minutes at room temperature. Meanwhile, a cell suspension of 8 x 10^5 cells/mL in RPMI media (0% FCS) was prepared. After the incubation period, reverse transfection was carried out by adding 25 μL of transfection mix into appropriate wells of a white polystyrene plate (Thermo Scientific Nunc F96 MicroWell White Polystyrene Plate), followed by addition of 50 μL of diluted cell suspension. The final volume of 75 μL per wells contained a total of 4 x 10^4 cells. The plate was incubated for 24 hours at 37°C in a humidified atmosphere of 5% CO_2 and 95% air.

Table 2.3: Total components of transfection mixture needed, on a per well basis, for each condition to be tested. No extra amounts compensating pipetting errors included.

Cignal Reporter	Cignal Negative Control	Cignal Positive Control	Specific miRNA	Negative Control siRNA	Nucleic Acid Mix	Attractene	Attractene Mix	time
100 ng (1.0 μL)				2 pmol	12.5 μL	0.6 μL	12.5 μL	
100 ng (1.0 μL)			2 pmol		12.5 μL	0.6 μL	12.5 μL	
	100 ng (1.0 μL)			2 pmol	12.5 μL	0.6 μL	12.5 μL	24 h
	100 ng (1.0 μL)		2 pmol		12.5 μL	0.6 μL	12.5 μL	
		100 ng (1.0 μL)			12.5 μL	0.6 μL	12.5 μL	

When aiming for induction using IL-1α, cells were stimulated after the initial incubation period of 24 hours with differing concentrations of agent and returned to the incubator for additional 4 hours (see 2.2.2.3). Therefore, in these experiments measurement of luminescent signal was performed 28 hours after transfection.

2.2.4 Measurement of luminescent signal

Quantitative assessment of luminescent signal produced by cells containing the transfected genes for firefly and *Renilla* luciferase was carried out using the Dual-Glo© Luciferase Assay System (PROMEGA). It is comprised of two reagents, the Dual-Glo© Luciferase Reagent which serves as substrate for the firefly luciferase and the Dual-Glo© Stop & Glo Reagent which quenches the firefly signal and simultaneously poses as substrate for *Renilla*.

Dual-Glo© Luciferase Reagent was aliquoted and stored at -70°C. Upon need, it was thawed on ice and 75 μL (equal to the total volume in a well) added to each well. Measurements using a luminometer (integration time of 1000 ms) were conducted after 10 min at room temperature. For assessment of the *Renilla* signal, 75 μL of freshly prepared Dual-Glo© Stop & Glo Reagent (substrate diluted 1:100 with

enclosed buffer) was added to each well and measured after an incubation period of 10 min at room temperature. Luminometer settings were not altered for the second measurement.

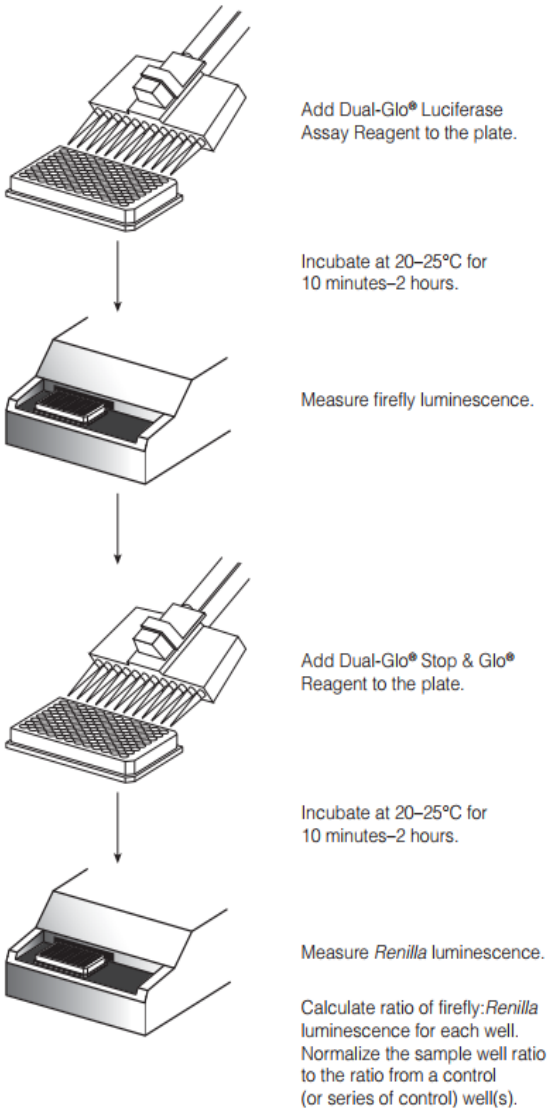

Figure 2.6: Schemativ representation of measurement procedure using the Dual-Glo© Luciferase Assay

2.2.5 Normalization of data

Constitutive expression of *Renilla* luciferase coupled with inducible firefly elements, allows for normalization of measured signals. This allows for compensation of varying transfection efficiencies and significantly enhances assay robustness. According to formula 2.1 (page 18), simple calculation of the ratio between firefly and *Renilla* can be used for inter- and intra assay comparison. Outliers were detected using the Grubbs test with a significance level of α=0.05.

To efficiently compare regulatory effects of transfected RNA, cells transfected with non-targeting control siR were taken as baseline. It was observed, that baselines between experiments differ to a non-negligible amount. To facilitate direct comparison of cell lines and normalize the natural variations amongst experimental replicas, the baseline signal was taken as 100% and all other setups expressed in relation thereof. This way, miRNA suspected to have repressing effects on NF-κB should deliver values below 100% (100%), whereas miRNA with stimulating abilities would show percentages above this arbitrary baseline (100%).

2.3 Criteria for mimic-miRNA and siR selection

2.3.1 Anti-RelA-siR

Validation of successful non-coding RNA transfection was established by including a positive control, ideally exhibiting potent NF-κB regulating abilities. Therefore, siRNA directly targeting the p65 subunit of NF-κB was chosen, which was purchased from Ambion (Carlsbad USA; ID# s11914, cat.no.: 4390824). Respective siRNA targets three of the four known transcript variants of p65 (variant 1, 2 and 4), as well as additionally two predicted by genomic sequencing. As corresponding non-targeting negative control, Silencer Select Negative Control No. 1 siRNA was chosen (Ambion; cat.no.: 4390843). According to the manufacturer, this negative control does not interfere in gene expression of any known genes, as validated by micro array analysis.

2.3.2 miR-mimetic

In order to evaluate the impact of specific miRNAs on metabolic pathways, synthetic miRNA, so-called miR-mimetics, can be transfected into the cell. Numerous different miRNA have already be identified to play a role in regulating the NF-κB signaling pathway [60, 61]. The approach for selecting a set of miRNA used in this thesis is based on the knowledge, that particular genes show a differential expression pattern depending on the degree of resistance to the chemotherapeutic agent [6]. It was concluded, this hints at possible divergences in miRNA abundances, which may act as regulatory elements. To test this hypothesis, a microRNA array was performed for both native cell lines (CCL228, CCL227) and all their resistant subgroups (low, intermediate and high resistant). The array was performed by Exiqon (Denmark) and included 3100 capture probes targeting all microRNAs for human, mouse or rat

registered in the miRBASE 18.0.

The heat map diagram (figure 2.7) shows the result of a two-way hierarchical clustering of miRNAs and samples. Colors illustrate the relative expression levels of miRNAs, with red representing lower and green higher expression in regard to the reference channel. It is evident, that numerous miRNAs show differing levels in the primary cancer cell line CCL228, which is also most susceptible to treatment with 5-FU [12].

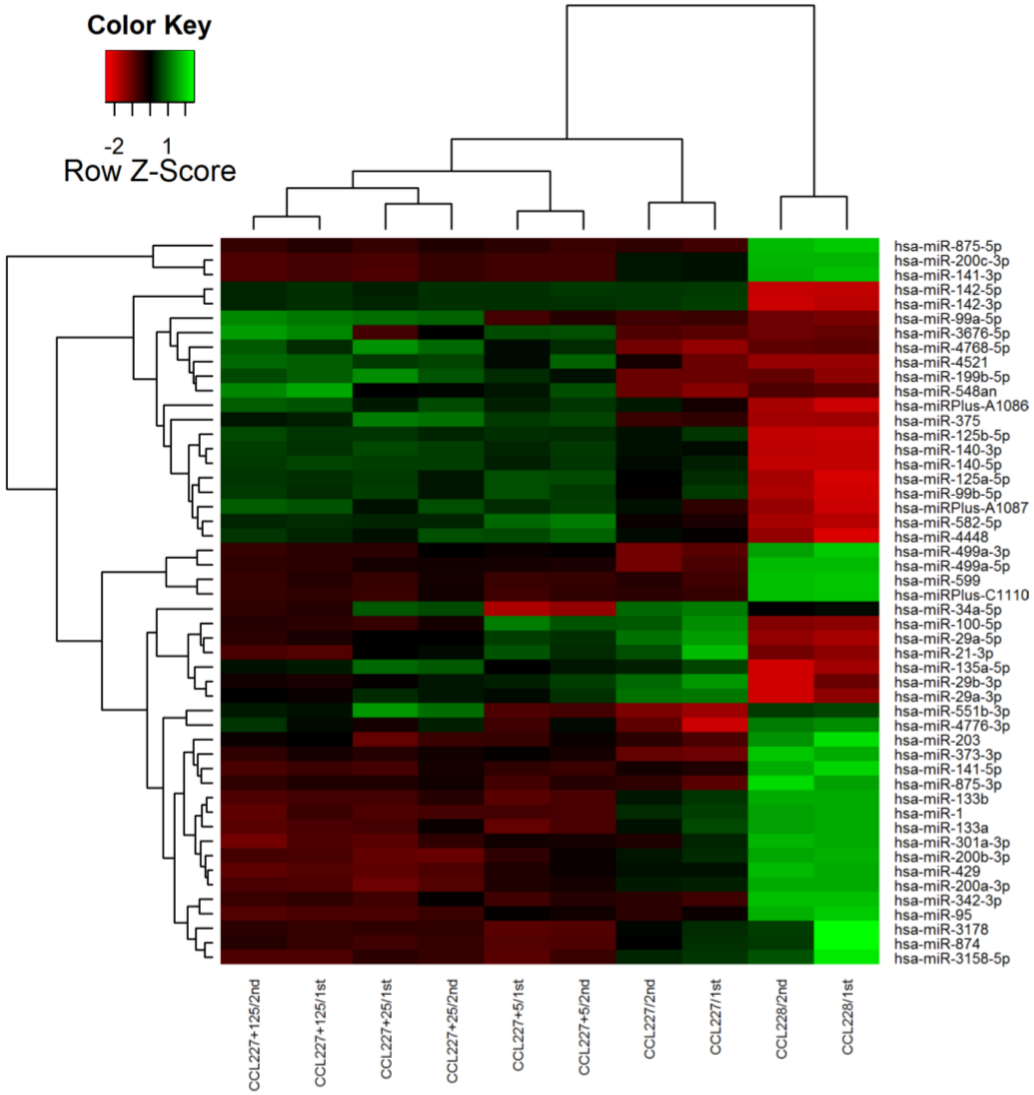

Figure 2.7: Heat Map and Unsupervised Hierarchical Clustering. The clustering was performed on all cell lines (duplicates), and on the top 50 microRNAs with highest standard deviation.

The nine top differentially expressed miRNA were obtained by sorting for relative differences in expression levels of the high resistance phenotype and CCL228 (figure 2.8).

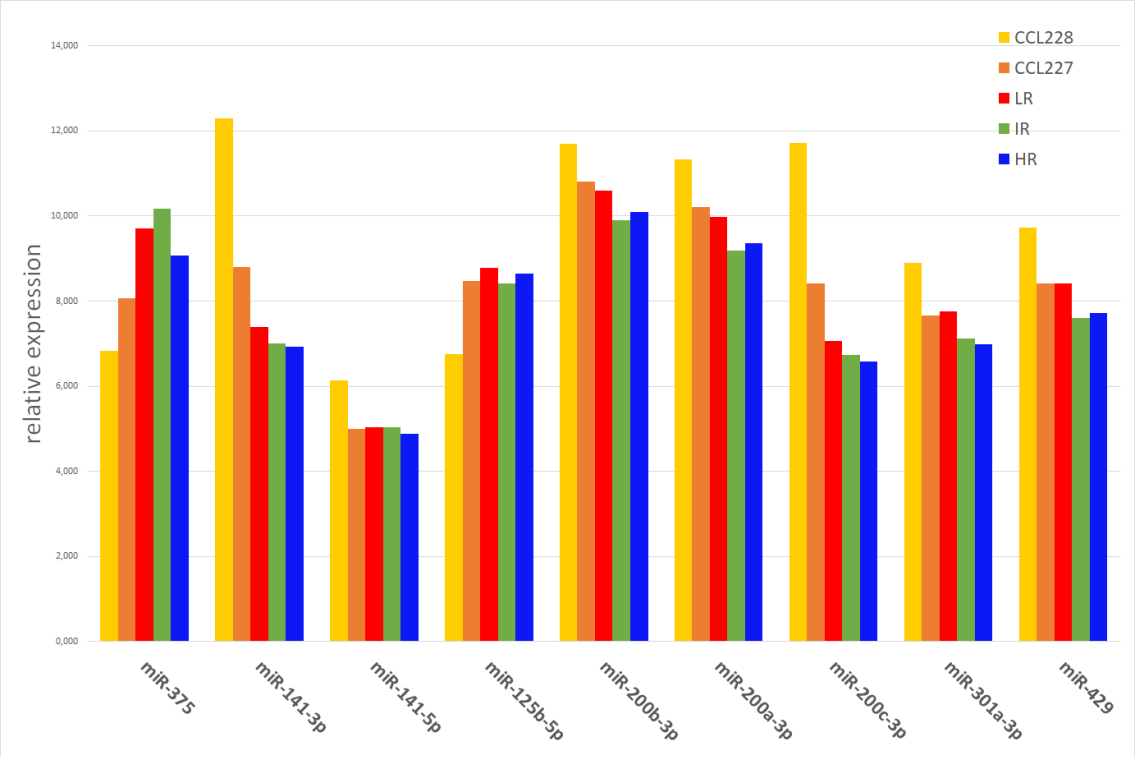

Figure 2.8: Top nine differentially expressed miRNA in each cell line (yellow: CCL228, orange: CCL227, red: low resistance, green: intermediate resistance, blue: high resistance)

Based on the significantly higher expression of NF-κB in resistant subclones compared to their native cell lines, the top differentially expressed miRNA depicted in figure 2.8 are suspected to play a role in regulation of the canonical/non-canonical NF-κB signaling pathway [12]. Highly expressed miRNA in the high resistant clones are therefore considered potential activators of the transcription factor, such as miR-375 or miR-125b-5p. In case of miR-141-3p or miR-200c-3p, expression is elevated in cell line CCL228, suggesting inhibiting capabilities. Going in accordance with this observation, studies have already shown the NF-κB upregulating capabilities of miR-125b, which even resulted in an increased resistance to radiotherapy in a nasopharyngeal carcinoma [60]. Also the inhibitory effects of miR-141 and miR-200c have been demonstrated, with the latter being a powerful enhancer of radiosensi-

tivity and currently in pre-clinical studies [57, 62]. Additionally, deregulation of respective miRNAs in the blood is believed to be able to serve as a prognostic tool when identifying breast cancer [63].

For this thesis, three miRNAs were chosen for more detailed analysis and transfection experiments: the potential downregulating miR-141-3p, upregulating miR-375 and miR-125b-5p. All of them were purchased from QIAGEN (miScript miRNA 141/375/125b). As negative control for miRNA transfections, the from the manufacturer suggested AllStars Negative Control siRNA (QIAGEN, cat. No. SI03650318), was used.

2.4 RT-qPCR analysis of cellular p65-mRNA and different miRNAs

When studying a protein of interest, most conventionally used methods aim to quantify protein levels directly, such as reporter studies or selective staining (immunoplotting) [64]. Such methods often neglect splicing patterns or post-transcriptional regulation mechanisms, for they are purely based on protein abundancy. By extending the analysis to the transcript level and comparing mRNA levels to effective protein concentrations, important conclusions regarding regulatory mechanisms can be drawn. This is especially interesting when artificially altering miRNA levels, because they exclusively act on the transcriptome, with the potential to repress translation or even induce mRNA degradation [65]. Examination of transcriptional levels of p65-mRNA was done by conducting RT-qPCR experiments subsequently to transfection of miRNAs. Additionally, successful miRNA transfection was validated using complementary primer sets.

2.4.1 Transfection of cell lines used for RT-qPCR

Ensuring that cells used for RNA isolation are treated identically to cells used for luminescent measurement, transfections included a reporter construct and were carried out under identical conditions. The procedure used differed from the protocol described in section 2.2.3 only in scale. The original manual featuring 4 x 10^4 cells per transfection was upscaled in order to work with a total of 2 x 10^5 cells without shifting ratios between reagents used. Therefore, all volumina depicted in table 2.3, were taken 5 fold (see table 2.4). Additionally, the Cignal Positive Control was chosen as reporter construct. By doing so, visual analysis of transfection success using a fluorescent microscopy was facilitated. The lack of an inducible promotor element featuring NF-κB binding sites in the Cignal Positive Control was no concern, because no luminescent measurements were carried out.

Table 2.4: Transfection setup prior to RNA isolation: total components needed, on a per well basis, for each condition to be tested. No extra amounts compensating pipetting errors included.

Cignal Reporter	Cignal Negative Control	Cignal Positive Control	Specific miRNA	Negative Control siRNA	Nucleic Acid Mix	Attractene	Attractene Mix	time
		500 ng (5.0 μL)			57 μL	9 μL	178.5 μL	
		500 ng (5.0 μL)		10 pmol	57 μL	9 μL	178.5 μL	24 h
		500 ng (5.0 μL)	10 pmol		57 μL	9 μL	178.5 μL	

2.4.2 Isolation of RNA

For RNA isolation, TRI REAGENT (SIGMA, cat.no. T 9424) was used. Before lysis, the supernatant medium was removed and 200 μL of TRI REAGENT directly applied on the cells. The cells were lysed immediately, and the resulting suspension transferred in PP-tubes, which were incubated for 5 minutes at room temperature. Subsequently, 50 μL of chloroform (SIGMA) was added and the tubes vortexed for

15 seconds. After 15 minutes of incubation at room temperature, the tubes were centrifuged at 12000 x g for 15 minutes at 4°C. Three phases were visible by then, the first phase being colorless and watery (RNA phase), the second phase being whitish (DNA phase) and the bottommost phase being the organic, red colored protein phase. After transfer of the RNA phase to a fresh PP-tube, 100 μL of chloroform were added and the sample tilted for 5 minutes. Subsequently, the tubes were centrifuged with the same settings as before (12000 x g, 15 minutes, 4°C). The watery phase was then transferred to a new tube. For precipitation of the isolated RNA 100 μL isopropanol (SIGMA) was added and the resulting solution incubated for 10 minutes at room temperature, before being centrifuged with the same settings as before (12000 x g, 15 minutes, 4C). The supernatant was removed and the pellet washed with 200 μL of 75% ethanol (Emprove). Therefore, the pellet in ethanol was vortexed well and centrifuged subsequently at 12000 x g and 4°C for 10 minutes. The supernatant was discarded and the pellet dried at room temperature for 10 minutes. Then, the pellet was dissolved in 10 μL of H_2O DEPC.

For further purification, the RNA was precipitated for 72 hours, using a precipitation solution (3 M sodium acetate - 1:10 diluted in ethanol absolute pH 5.5). The sample was substituted with water to 50 μL, 150 μL of precipitation solution was added (50 μL = ratio of 1:3) and mixed by pipetting. The tubes were stored at -20°C and subsequently centrifuged for 30 minutes at 15000 rpm and 4°C, the resulting pellet dried at room temperature and was resuspended in 10 μL of DEPC-H_2O. At this point, the concentration of the isolated RNA was measured using the NanoDrop photometer. The isolated RNA samples were stored at -80°C and were concentrated enough to be used for a number of RT-qPCR analysis.

2.4.3 Unspecific cDNA synthesis

The isolated and purified RNA was reversely transcribed to cDNA, using the miScript II RT Kit from QIAGEN (cat.no. 218161). A master mix (MM) according to table 2.5 was prepared, using the reagents supplied in the Kit. 10 μL of master mix sufficed for one sample. 10 ng absolute RNA content of RNA extracted prior (section 2.4.2) was diluted in 5 μL RNase-free water (=2 ng/μL) and transferred into a SoftTube. The master mix was pipetted according to scheme, spun down briefly and mixed my pipetting. 10 μL of the master mix were then transferred into each SoftTube already containing 5 μL diluted sample (2 ng/μL) or 5 μL RNAse-free H_2O (negative control). Subsequently, the tubes were sorted into the Thermo Hybaid PCR EXPRESS (Thermo Scientific). Program settings for the PCR-run included a preheating phase of 60 minutes at 37°C, the denaturation step at 95°C for 5 minutes and subsequent temperature hold at 4°C until the tubes were removed from the thermocycler. The newly synthesized cDNA was stored at -20°C.

Table 2.5: cDNA master mix scheme. Displayed volumina are depicted per sample. No extra amounts compensating pipetting errors included.

reagent	concentration	μL/tube
miScript HiFlex Buffer	5x	3
miScript Nucleics Mix	10x	1.5
RNase-free water	-	4
miScript Reverse Transcriptase Mix	-	1.5
		10 μL MM
		+ 5 μL RNA sample (2 ng/μL) or H_2O
	total reaction volume	15 μL

2.4.4 Reverse transcription - quantitative PCR (RT-qPCR)

Reverse transcription (RT) followed by polymerase chain reaction (PCR) has been the golden standard for mRNA quantification for many years [66].

The simple, but very sensitive detection method used bases on the binding ca-

pacity of SYBR Green I fluorescent dye to the minor groove of the newly synthesized double-stranded DNA. By using designed primers to specifically enrich the construct of interest and measuring increasing fluorescence levels over time, originally present mRNA levels can be deduced [67].

2.4.4.1 RT-qPCR primers

In order to facilitate quantification of p65-mRNA, two different primer pairs were used, both acquired from QIAGEN (QuantiTect Primer Assay, product no. 249900). The Hs_RELA_1_SG QuantiTect Primer Assay (abbrv. RelA1, cat. no. QT01007370), as well as the Hs_RELA_2_SG QuantiTect Primer Assay (abbrv. RelA2, cat. no. QT02324308) detect four, and therefore all known transcripts of RelA. The difference between those primers is the length of amplified construct, with RelA1 exhibiting a final transcript length of 107 nt, and RelA2 of 136 nt. Due to the increased length of RelA2, six of the seven exons (number according to Ensembl Transcript) are amplified, which can be related to a very good overall coverage of the p65 gene, including all known, as well as most splicing variants predicted by next-generation sequencing.

A potent validation of transfection success is quantification of transfected constructs using qPCR. In this work, efficient miRNA transfection was confirmed using cells transfected with miR-375 mimetics and primers specific for cellular mature miR-375 (QIAGEN, miScript Universal Primer, product no. 218300, cat. no. MS00031829).

The mathematical model chosen to describe data obtained from each qPCR experiment, calls for normalization using a reference gene, to ensure robust results [68]. This endogenous standard should not be affected by regulatory mechanisms, to ensure stable expression. As so-called "housekeeping gene", RNU48, also known as SNORD48 (small nucleolar RNA, C/D box 48) was used. Primers were acquired from QIAGEN (miRCURY LNA miRNA PCR Assay, product no. 339306, cat. no.

YP00203903).

2.4.4.2 RT-qPCR sample preparation

qPCR experiments were conducted using the QIAGEN miScript SYBR Green PCR Kit (cat. no. 218073). This kit consists of the QuantiTect SYBR Green PCR Master Mix and the miScript Universal Primer, which is a reverse primer that allows detection of miRNAs in combination with one of the primers described in section 2.4.4.1. In case of aiming to detect RelA levels, the miScript Universal Primer does not have to be added, because both primers, forward and reverse, are included in the QuantiTect Primer Assay. All experiments were carried out as quadruple assay to be able to run statistical tests, providing confidential results. The instrument of choice for real-time cycling was the Rotor-Gene Q (QIAGEN).

Firstly, synthesized cDNA prepared according to 2.4.3 was diluted 1:100 using RNase-free water (1 μL cDNA + 99 μL RNase-free water). Depending on the to total number of samples, the amount of master mix needed was calculated including additional extra to account for any pipetting errors. Volumes per tube are depicted in table 2.6.

Table 2.6: qPCR master mix scheme. Displayed volumina are depicted per sample. No extra amounts compensating pipetting errors included.

reagent	conc.	μL/tube
QuantiTect SYBR Green PCR Master Mix	2x	5
miScript Universal Primer*	10x	1
miScript Primer Assay	10x	1
RNase-free water	-	1.67
		8.67 μL MM
		+ 1.33 μL cDNA (1:100) or H_2O
	total reaction volume	10 μL

* added only when using miR-375 or RNU48 primers

The Rotor-Gene Q loading block was precooled at 4°C and equipped with strip tubes (QIAGEN, cat. no. 981103). 1.33 μL of sample cDNA was pipetted on the

wall of each tube (for negative control: 1.33 μL RNase-free water). Subsequently, 8.67 μL of respective master mix was added, dragging the droplet down whilst pipetting. The tubes were closed off with fitting caps and loaded into the rotor disc. Empty slots were filled up with empty tubes/old samples to prevent imbalance. Program setting of the Rotor-Gene Q were as follows:

- Hold: 15 min - 95°C
- Cycling:
  - Denaturing: 15 sec 94°C
  - Annealing: 30 sec 55°C
  - Extension: 30 sec 70°C (+ "Acquire for Green,,)
- Cycle number: 40
- Melt:
  - Ramp from 50°C to 99°C
  - Hold for 90 sec on the first step
  - Hold for 5 sec on the next steps (+ "Acquire for Green,,)

2.4.4.3 RT-qPCR data analysis

For data analysis the provided Rotor-Gene Q Software 2.3.1.49 was used. It features three output formats, the quantification curve, amplification rate, and melt curve, which will be discussed shortly. Each output consists of a graphical visualization and a detailed table, summarizing results for each sample.

Figure 2.9 is an exemplary result of a quantification curve after normalization and slope correction. The red horizontal line indicates the arbitrary chosen threshold value of 0.02. The threshold fluorescence is defined as the point, at which measured

fluorescence rises considerably above the background signal. This reduces the chance of mistaking noise as measurement and therefore avoid overfitting of data. The cycle at which the fluorescent signal crosses the threshold is called "crossing point" (CP) or "cycle threshold" (CT). The later the sample exceeds the defined threshold (rising CT), the less specific RNA is present. This in turn, possibly corresponds to low gene expression. Therefore, the cycle threshold serves as base for all subsequent analysis steps with various mathematical models. It is noteworthy, that some lines do not cross the threshold. Samples corresponding to those lines derive from tubes containing old samples, which were merely used as counterweights and can hence be ignored.

Measured samples are color-coded, with one line referring to a distinct sample. Samples exhibiting CTs around 20 cycles derive from tubes containing amplified housekeeping gene RNU48, indicating a higher amount of cDNA relative to other samples.

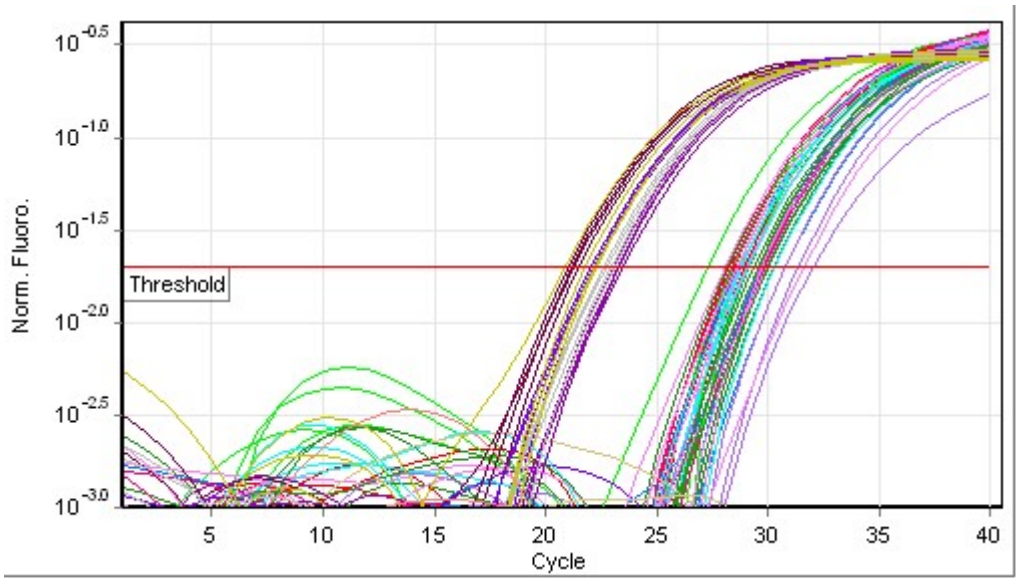

Figure 2.9: Example of a RT-qPCR quantitation curve after normalization and slope correction; each quadruple sample is colored individually. A threshold value of 0.02 was set prior to analysis.

To assess the quality of the performed RT-qPCR, two indicators can be used: the amplification rate and the melt curve. Theoretically, an amplification rate of 2.0 is ideal, although in practice rates above 1.7 are classified as successful. Low amplification rates hint at technical problems during the PCR run, in which case repetition of respective samples is advised.

Figure 2.10 shows a melting curve, which can be recorded after completing all amplification cycles. Therefore, the temperature is set to a starting temperature of 50°C and the samples heated gradually, accompanied by measurement of the fluorescent signal. It is important to note, that the dye used in RT-qPCR only fluoresce when bound to double-stranded DNA (dsDNA). By increasing the temperature, the dsDNA denatures, becoming single-stranded, which results in a decline of fluorescent signal. Subsequent plotting of change in the slope of this curve as a function of temperature results in the melting curve. Typical for such a curve is the presence of a single peak for each sample cDNA, displaying one specific denaturing temperatures, which can be regarded as prove for product purity.

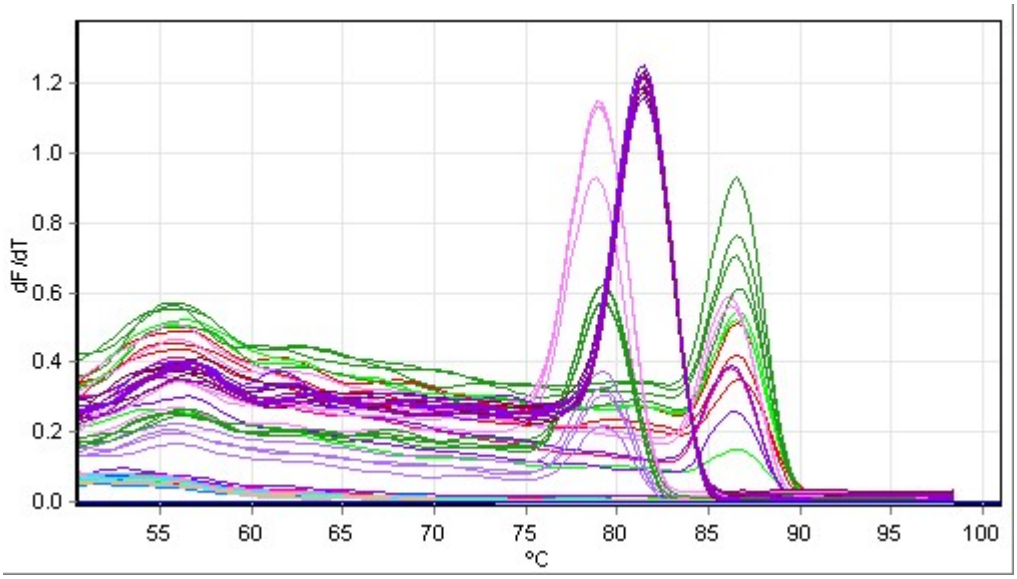

Figure 2.10: Example of a RT-qPCR melt curve; each quadruple sample is colored individually.

Even though RT-qPCR provides rapid and reliable quantification results, accurate comparison of experimental data requires a suitable mathematical model. The model of choice used in this thesis was established by M.W. Pfaffl [68]. It is a relative quantification approach, where the target gene transcript is compared to a reference gene transcript. This reference gene should show an unaltered expressional profile throughout all experimental treatments and methodological alterations. For this reason, non-regulated genes or so called "housekeeping genes" are chosen as reference. Here, RNU48, also known as SNORD48 (small nucleolar RNA, C/D box 48) was used.

The mathematical model derived by Pfaffl is depicted in equation 2.2.

$$\text{ratio} = \frac{(E_{target})^{\Delta CT_{target}(control-sample)}}{(E_{ref})^{\Delta CT_{ref}(control-sample)}} \tag{2.2}$$

The relative expression ratio of target gene in comparison to the reference is based on the transcript amplification efficiency (E) and the difference in CT of treated sample versus negative control ($CT(control - sample)$).

2.5 *In vitro* cell cytotoxicity assay

Monitoring the viability of cancer cells under different conditions is a vital part of oncological research and drug development. This is especially the case when working with a carcinoma model that exhibits resistance to a widely used therapeutic drug. Assessing the degree of resistance and impact of potential resistance modulating agents are mostly done by *in vitro* viability assays, such as the so-called MTT assay. It is based on the reduction of water-soluble yellow dye 3-(4,5-dimethylthiazol-2-yl)-2,5-diphenyltetrazolium bromide (MTT) to insoluble purple colored formazan [69]. Subsequent quantification is based on photometric measurement around the absorption maximum of formazan. The reaction is dependent on NADH-dependent oxidoreductase enzymes in the cytosolic compartments of the cell and therefore directly proportional to metabolic activity [70, 71]. The MTT assay is a popular tool for cytotoxicity testing of drug-resistant cell lines, as well as freshly isolated tumor samples [72, 73].

By using this assay, we aimed to detect whether regulation using non-coding RNA could have an impact on cell viability, in particular when transfecting p65-siR, which directly modulates one of the key players conferring drug resistance [12].

2.5.1 Transfection of cells used for viability determination

The original transfection protocol featured a cell count of 4 x 10^4 cells per well (see 2.2.3). This number has to be reduced when performing an assay using photometric measurements, due to the possibility of obtaining signals that exceed the instrument's linear range. The MTT protocol used for native cells suggests a cell count of 5000 cells per well but because of the increased mortality upon transfection the cell count was increased to 10000 (1 x 10^4) cells per well. The volumina described in 2.2.3 were altered accordingly and scaled down in order to be suitable for the

reduced amount of cells. The modified transfection scheme is illustrated in table 2.7. For the control wells containing untreated cells, a cell count of 5000 was maintained. Because no luminescent measurement of transcription factor activity was carried out, the Cignal Positive Control construct was used. This further allowed for visual analysis of transfection success by fluorescent microscopy.

Table 2.7: Transfection setup prior to MTT assay: total components needed, on a per well basis, for each condition to be tested. No extra amounts compensating pipetting errors included.

Cignal Reporter	Cignal Negative Control	Cignal Positive Control	Specific miRNA	Negative Control siRNA	Nucleic Acid Mix	Attractene	Attractene Mix	time
		25 ng (0.25 μL)		0.5 pmol	6.25 μL	0.15 μL	6.25 μL	24 h
		25 ng (0.25 μL)	0.5 pmol		6.25 μL	0.15 μL	6.25 μL	

2.5.2 MTT assay

When working with native cells:

Cells were cultivated in T75 flasks with RPMI 1640 media supplemented with Glutamax-I (Gibco) and 10% exosome-free fetal calf serum (FCS) (Sigma) at 37°C in a humidied atmosphere of 5% CO_2 and 95% air until confluency has reached approximately 80%. After washing of cells with an equvialent volume of 1x DPBS (Gibco) and detaching using 1x Accutase (Sigma), they were resuspended in media and centrifuged at 287xg for 5 minutes. The pellet was dissolved in fresh media and the cell concentration determined by counting in a thoma chamber. Subsequently dilutions of 5 x 10^4 cells/mL were established. 100 μL of these dilutions (corresponding to approximately 5000 cells) were added in triplets to a microtiter plate. Subsequently, the plates were wrapped in aluminum foil (to prevent dehydration) and incubated for 24 hours at 37°C and 5% CO_2.

When working with transfected cells:

Transfection procedure was identically to the protocol described in 2.2.3 with volumina depicted in table 2.7. The final volume in each well added up to be 62.5 μL (12.5 μL transfection mix + 50 μL cell suspension), with a cell count of 1 x 10^4 cells. Cells were incubated for 24 hours at 37°C and 5% CO_2.

A dilution series from the cytostatic 5-fluorouracil 60 mM stock solution (5-fluorouracil in physiological NaCl-solution) was prepared in a decimal series of seven dilution steps from 60 mM to 60 nM in RPMI media. After the initial incubation period of 24 hours, 25 μL of the appropriate 5-FU dilution was added to the cells. After complementing the volume in each well to a total of 150 μL with media (addition of another 25 μL to each well containing 5-FU; 50 μL to the negative control wells), the final concentration of 5-FU ranged from 10 nM to 10 mM (see table 2.8) Subsequently, the plates were re-wrapped in aluminum foil and returned to the incubator for another 144 hours, under the same conditions. After this extended incubation period, 15 μL of a MTT salt solution (Thiazolyl Blue Tetrazolium Bromide 98% in PBS) were added to in each well and the microtiter plate was again incubated (also wrapped) for 4 hours under the same conditions. Then 100 μL of solubilization solution (40% N,N-Dimethylformamid, 20% SDS; pH 4.5-5) were added and the wrapped microtiter plate left in the exhaust hood at room temperature for 24 hours. Measurement of the specific exctinction at 570 nm was performed with Biochrom Asys Expert Plus Microplate Reader (reference wavelength: 690 nm).

Table 2.8: Schematic representation of 96-well plate outlay for MTT assays. All experiments were carried out as triplets. A total of seven decimal concentration steps ranging from a final cytotoxic agent concentration of 10 mM to 10 nM per well were chosen.

	Sample A				Sample B				Sample C			
neg. control	→	→	→		→	→	→		→	→	→	
10 nM FU	→	→	→		→	→	→		→	→	→	
100 nM FU	→	→	→		→	→	→		→	→	→	
1 μM FU	→	→	→		→	→	→		→	→	→	
10 μM FU	→	→	→		→	→	→		→	→	→	
100 μM FU	→	→	→		→	→	→		→	→	→	
1 mM FU	→	→	→		→	→	→		→	→	→	
10 mM FU	→	→	→		→	→	→		→	→	→	

2.5.3 Data analysis

Data obtained from photometric measurement at the absorption maximum of formazan was analyzed using the GraphPad Prism 4.0 software. A dose-response curve was obtained by fitting data to a sigmoidal model (nonlinear regression curve fit). From the constructed curve the IC50 can be derived, which is defined as the concentration of cytotoxic agent at which 50% of the original present cells have deceased. Due to its quantitative and universal nature the IC50 is often used to compare the potency of drugs.

Experimental Results

3.1 Chemoresistance of colon carcinoma cells

The cell culture model system used for all experiments contained a set of five different cell lines, all classified as colon carcinoma cells. Primary adenocarcinoma CCL228 (also called SW480) and its lymph node metastasis CCL227 (SW620) were obtained from the ATCC. From cell line CCL227, three subclones with progressing resistance to the cytotoxic agent 5-fluorouracil (5-FU) were derived. Stepwise increase in the degree of chemoresistance was confirmed by identifying the effective concentration (IC50) using MTT assays.

Figure 3.1a a shows the non-linear regression model used to determine the IC50. A visual comparison of differences in resistance to 5-FU of all cell lines is given in figure 3.1b, with mean IC50 values depicted above each bar. Notable here is the decreased degree of resistance in CCL227 (figure 3.1b: orange bar) when compared to CCL228 (figure 3.1b: yellow bar). This observation can be accounted to the lower initial cell count, as seen in the decreased extinction around low 5-FU concentrations (figure 3.1a).

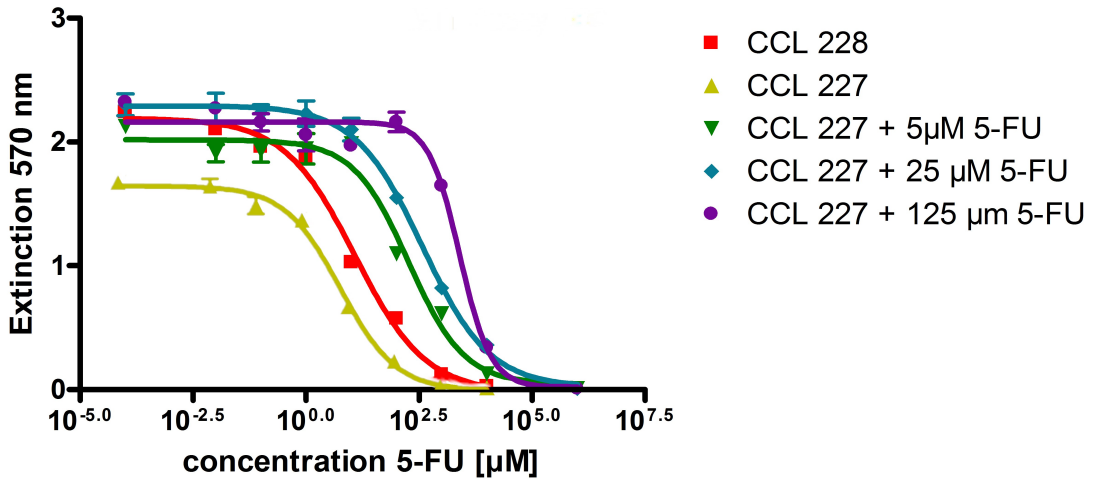

(a) Dose-response curve (mean±S.D.) after exposure to increasing concentrations of 5-FU. Data analyzed by GraphPad Prism 5. A non-linear regression was calculated using sigmoidal dose-response curve analysis with variable slope to determine the IC50.

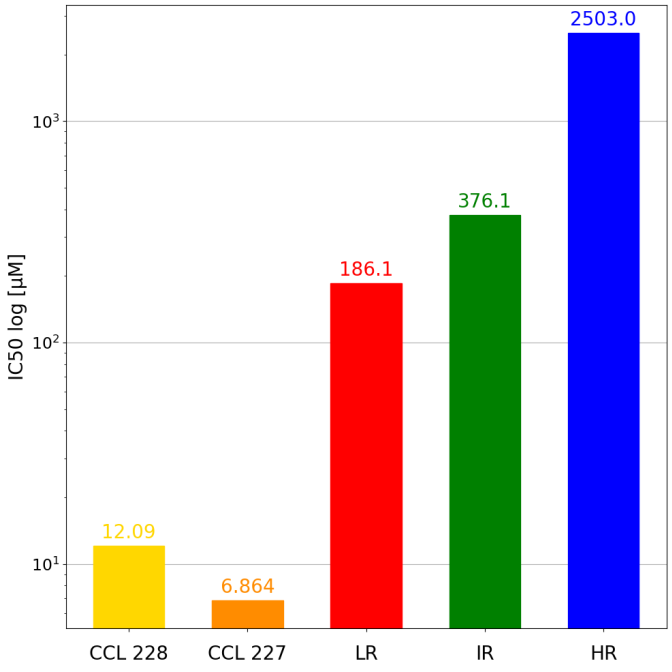

(b) Overview of IC50s determined in 3.1a. Detailed IC50 values ([μM]) for each cell line are depicted above corresponding bars.

Figure 3.1: Stages of chemoresistance in CCL228 (yellow), CCL227 (orange), the low-resistance (LR; red), intermediate-resistance (IR; green) and high-resistance (HR; blue) phenotypes.

3.2 Transfection of reporter plasmid: Qualitative and quantitative analysis

Reporter assays heavily depend on efficient transfection of cells with the plasmid constructs harboring the reporter gene. The overall transfection setups are suggested by the manufacturer but are very cell line dependent, demanding alterations in order to be fully effective. This sometimes requires trial and error testing of different influential factors, which makes a tool for qualitative assessment of transfection efficiencies indispensable.

In this work, successful transfection of the reporter into the cells was evaluated using the positive control construct ,,Positive Cignal Reporter" (referred to as ,,Cignal Positive"), provided by the manufacturer. The Cignal Positive control is based on the additional expression of green fluorescent protein (GFP), facilitating visual control by fluorescence microscopy (see figure 3.2). Every experiment conducted included transfection of positive control and qualitative evaluation of GFP expression prior to further measurements. Although no quantification of fluorescent protein was carried out, comparison of GFP abundance in each cell line allows for conclusions concerning transfection efficiencies. As an example, figure 3.2 depicts fluorescent microscopy images of cell line CCL228 and the high-resistance phenotype 24 hours after transfection procedures. The resistant subclone (3.2b) exhibits notably less fluorescence than its mother cell line CCL228 (3.2).

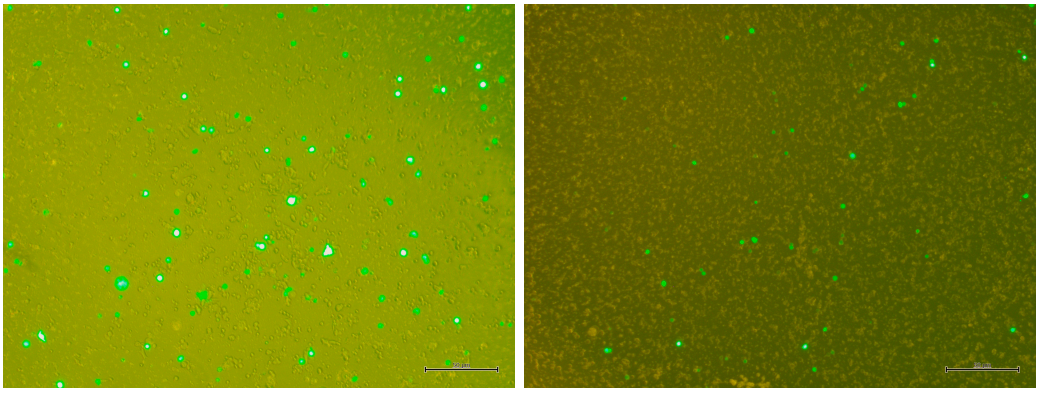

(a) CCL228 (b) High-resistance phenotype

Figure 3.2: GFP expression of cell lines CCL228 and the high-resistance phenotype transfected with the ,,Positive Cignal Reporter". Fluorescent microscopy pictures taken 24 hours after transfection. Cells harboring fluorescent GFP are visible as light green spots.

As a quantitative approach to estimate transfection success, evaluation of efficiencies is achieved by comparison of *Renilla* luciferase levels observed in all cell lines. The ,,Cignal" reporter construct transfected for determination of NF-κB levels features a constitutionally expressed *Renilla* luciferase, used for normalization of the obtained signals and compensation of varying transfection efficiencies (see 2.2 for further information). *Renilla* intensities are therefore directly proportional to the number of transfected cells and can be related to transfection success. Figure 3.3 shows all cell lines with their *Renilla* signal intensities 24 hours post transfection. Going in accordance with visual analysis of GFP expression, CCL228 exhibits the highest number of transfected cells. Light intensities for residual cell lines are similar, with the highly resistant cell line showing a rather unstable signal, as depicted by the large error bar.

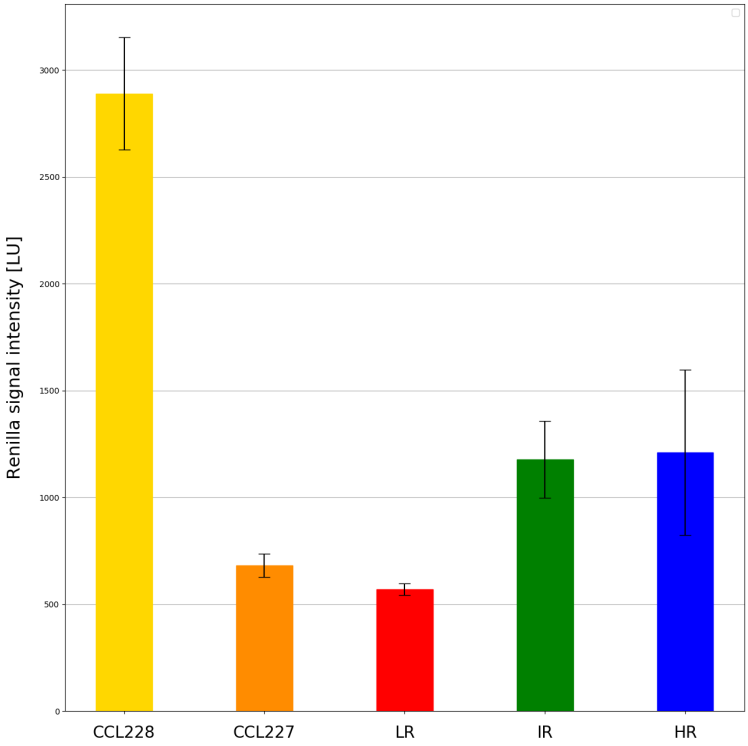

Figure 3.3: Average *Renilla* signal intensities of the primary tumor CCL228, parental cell line CCL227, the low-resistance (LR; with 5 μM 5-FU), intermediate-resistance (IR; with 25 μM 5-FU) and high-resistance (HR; with 125 μM 5-FU) phenotype. Mean and standard deviations depicted is representative for two independent experiments, performed in triplicates.

3.3 Determination of NF-κB baselines

Correlations between observed resistance to 5-FU and NF-κB activation included comparison of baseline NF-κB levels in all cell lines. Therefore, the ,,Cignal" reporter construct was transfected into native cells and luciferase levels measured subsequently. A visual representation thereof is shown in figure 3.4. Whilst the primary carcinoma (CCL228, yellow) and one replica of the metastatic cell line (CCL227, orange) show low abundancy of the transcriptional factor, an increase in resistance to 5-FU up to 25 μM results in a profound elevation of NF-κB (LR: red, IR: green).

Very interestingly, the high-resistance phenotype shows expressional levels similar to CCL228, despite a 5-fold increase in resistance compared to the former resistance stage. Notable as well is the inhomogeneity amongst the CCL227 replicas, as well as overall high standard deviations. This hints at an easily perturbed signaling pathway which may be dependent on cell age and growth conditions.

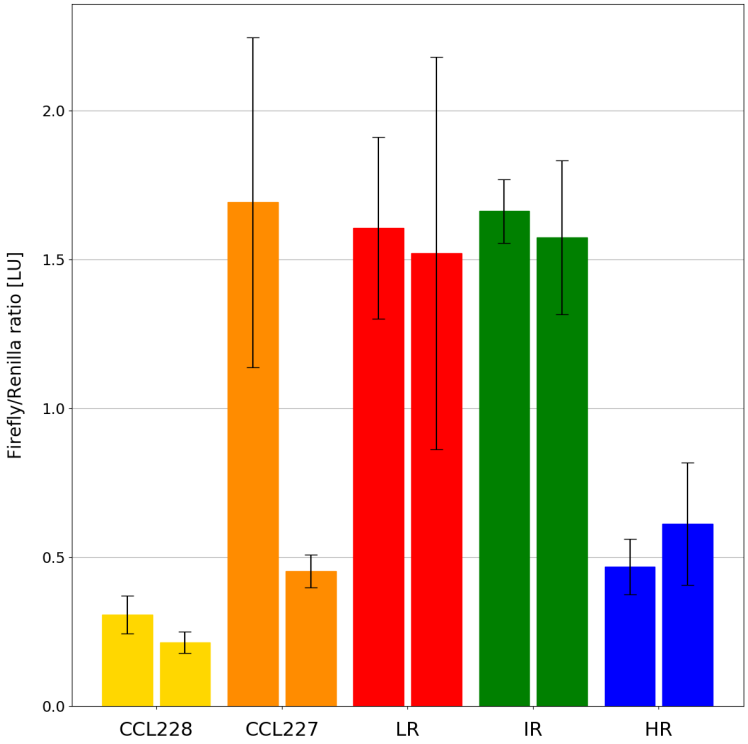

Figure 3.4: Luciferase activity relatable to NF-κB activation. Cell lines investigated included the primary carcinoma CCL228, its metastasis CCL227 and all resistant subtypes (low-resistance: LR, intermediate-resistance: IR, high-resistance: HR). Mean and standard deviations depicted derived from two biological replicas, performed in triplicates.

In an attempt to elevate native NF-κB levels, CCL227 was stimulated with varying concentrations of α-IL-1 4 hours prior to measurement (see table 3.1). Regardless of the concentrations used, no significant rise in NF-κB could be detected (figure 3.5). Even unphysiologically high concentrations of 1 ng/mL (1000 pg/mL) up to

100 ng/mL (100.000 pg/mL) did not elevate protein levels by more than a factor of 1.78.

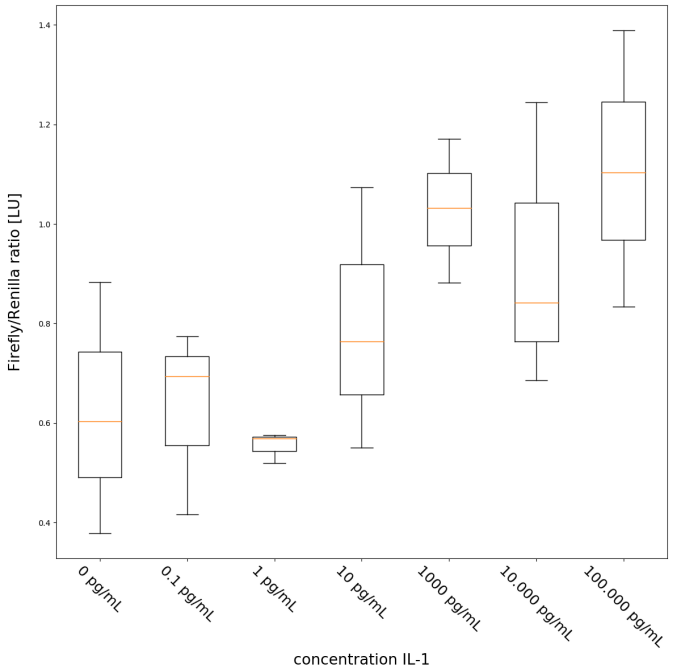

Figure 3.5: Luciferase activity after treatment of CCL227 using NF-κB stimulating α-IL-1 in concentrations from 0.1 pg/mL - 100.000 pg/mL. Medians are depicted as orange horizontal lines and whiskers correspond to the 95% confidence intervals. Data shown was derived from two independent experiments, performed in triplicates.

Table 3.1: Summary of average change in of luciferase activity upon treatment of CCL227 with α-IL-1 (see figure 3.5). Measurements were conducted 4 hours after induction. Fold increases depicted are calculated relative to 0 pg/mL α-IL-1 (unstimulated cells).

Concentration of α-IL-1 [pg/mL]	0	0.1	1	10	1000	10.000	100.000
Fold increase of luciferase activity	-	1.01	0.89	1.28	1.65	1.49	1.78

3.4 Impact of p65-siRNA on the NF-κB signaling pathway

Studying the potential of non-coding RNAs as regulating elements on the post-transcriptional level requires knowledge on their maximal efficacies and limitations. Therefore, transfections using siRNA selective for the p65 subunit of NF-κB (p65-siR) were conducted. It is to be expected, that siRNA directly compatible to one of the transcription factor elements, is highly potent and able to efficiently alter protein levels.

The NF-κB suppressing capabilities of this siRNA are clearly visible in all cell lines (figure 3.6). Independent of the degree of resistance, p65-siR is able to efficiently lower NF-κB levels up to 65%, as in the case of CCL227 (orange bar). The degree of NF-κB suppression seems to be independent from the stage of resistance.

In order to explore the inhibiting capacities further and highlight concentration dependent effects, varying concentrations of p65-siR were transfected in the low-resistance cell line (LR) and the luminescent signal evaluated (figure 3.7). It is visible that the potency of p65-siR does not diminish upon lower concentrations. A dilution of siR solution by a factor of 5 (5 μM) is able to downregulate NF-κB as efficiently. Several experiments included unphysiologically high concentrations of p65-siR of up to 266 nM (data not shown). Concentrations this high resulted in an overstimulation of the cells, apparent as a decrease of the downregulating capabilities of the siRNA.

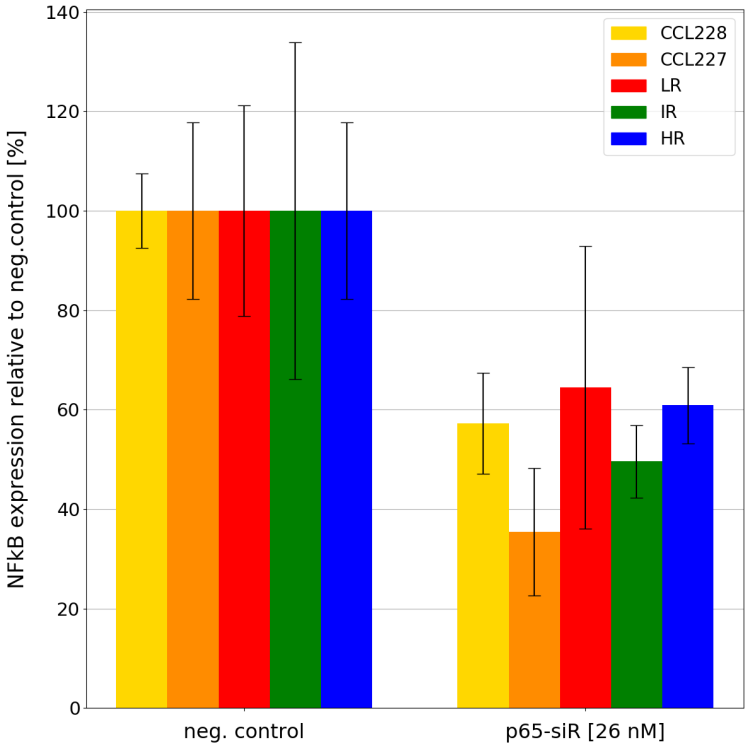

Figure 3.6: Impact of p65-siR transfection on parental cell lines CCL228, CCL227 as well as low-resistant (LR, with 5 μM 5-FU), intermediate-resistant (IR, with 25 μm 5-FU) and high-resistant (HR, with 125 μM 5-FU) subclones. NF-κB expressions are depicted relative to cells transfected with negative control siRNA (neg. control). Results are representative of two independent experiments, performed in sextuplicate.

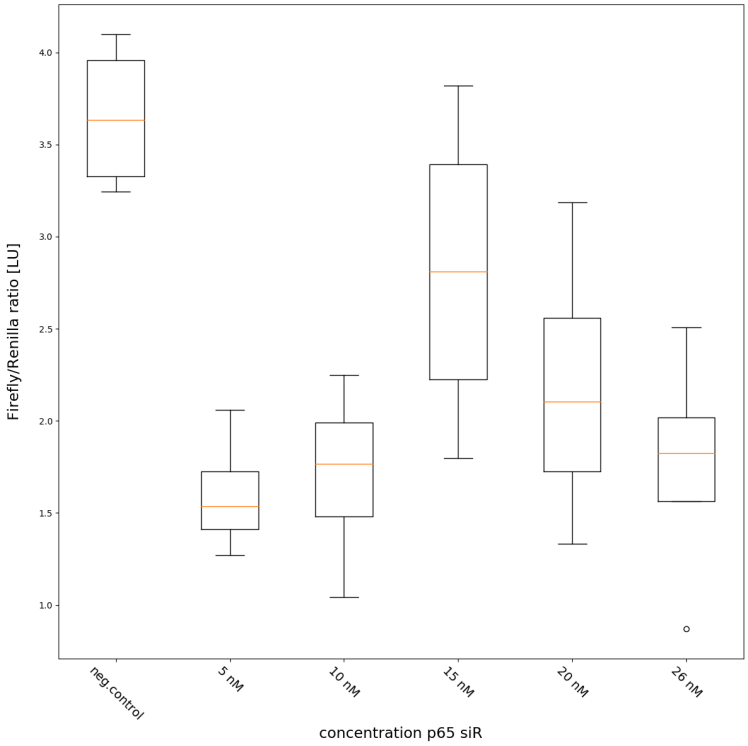

Figure 3.7: Normalized luminescent signal after transfection of the low-resistant phenotype with varying p65-siR concentrations (5 nM - 26 nM). Medians are depicted as orange horizontal lines and whiskers correspond to the 95% confidence intervals. Data shown was derived from two independent experiments, performed in sextuplicate.

3.5 Impact of selected miRNA on the NF-κB signaling pathway

Differences in expression patterns of miR-141, miR-375 and miR-125b between the native cell lines and resistant subclones led to the hypothesis of them being potential regulators of NF-κB expression (see 2.3). The overexpression of miR-375 and miR-125b in resistant subclones was suggested to be involved in the inflammatory activation observed. Vice versa, miR-141 levels proved to be elevated in 5-FU susceptible cell lines, maybe conferring tumor suppressor capacities by lowering ma-

lignant NF-κB levels. It was concluded, that transfection of miR-375 or miR-125b with assumed stimulating capabilities, or miR-141 with its suppressing properties, might lead to measurable changes in NF-κB abundance. These changes were sought to be quantified using the luminescent assay described before. In addition to these, p65-siR was included in each experiment due to its strong downregulating abilities, posing as a direct comparison and positive control.

As seen in figure 3.8, none of the selected miRNA was able to significantly and reliably modulate the NF-κB signaling pathway. Whereas miR-141 shows a slight suppressing effect in all cell lines, it cannot be compared to the potency of p65-siR. MiR-375 exhibits stimulating abilities, although they seem to be cell line dependent and difficult to reproduce consistently. MiR-125b fails to induce any noteworthy rise in signal. Interestingly, for most cell lines transfected with miR-375 and for all cell lines with miR-125b, a decrease in signal equivalent or greater than miR-141 is observed. Generally, all samples suffered from high intra-assay variations. However, experimental replicas conducted at different points in time showed similar results as described above.

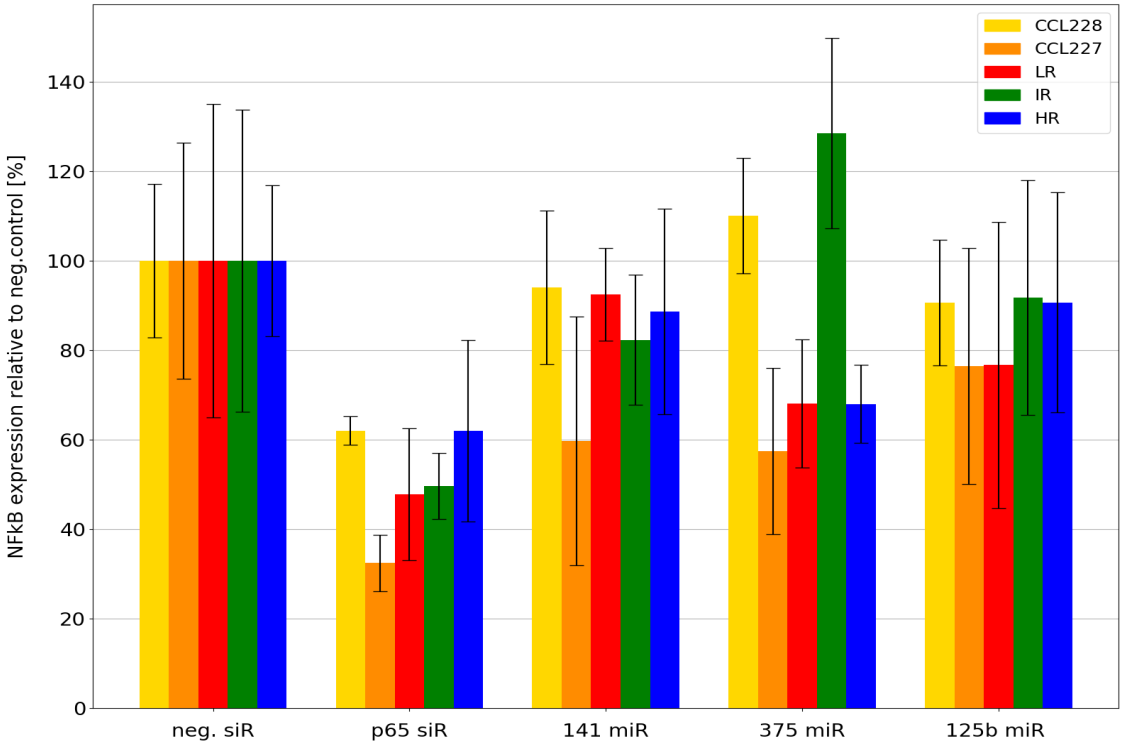

Figure 3.8: Overview on transfection of a selection of miRNA (p65-siR, miR-141, miR-375, miR-125b) in the parental cell lines CCL228 and CCL227, as well as low-resistant (LR, with 5 μM 5-FU), intermediate-resistant (IR, with 25 μm 5-FU) and high-resistant (HR, with 125 μM 5-FU) subclones. NF-κB expressions are depicted relative to cells transfected with negative control siRNA (neg. siRNA). Data shown was derived from two independent experiments, performed in sextuplicate.

A potential cause for the adverse effects exhibited by the stimulating miRNAs is overstimulation of the cells. To test this, miR-125b in lower ranging concentrations was transfected into cell line CCL227 and luminescent signal ratios derived (figure 3.9). None of the selected concentration steps was able to stimulate NF-κB expression, supporting results shown in figure 3.8 and eliminating concerns regarding negative effects on transfections using concentrated miRNA solutions.

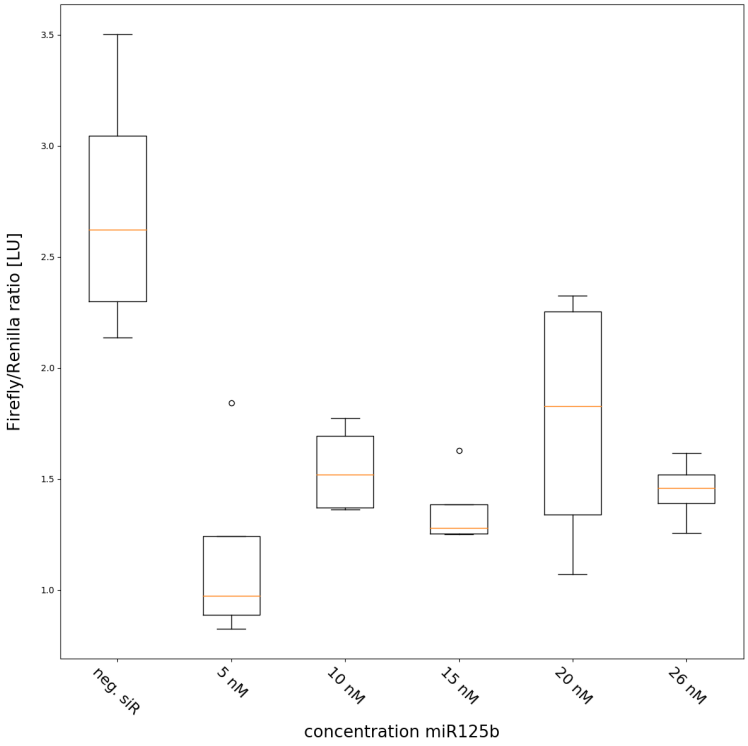

Figure 3.9: Ratio of luminescent signals transfection of the low-resistant phenotype (LR) with varying miR-125b concentrations (5 nM - 26 nM). Medians are depicted as orange horizontal lines and whiskers correspond to the 95% confidence intervals. Data shown was derived from two independent experiments, performed in sextuplicate.

3.6 RT-qPCR analysis

The luminescent reporter system described so far delivers an insight on abundances of the transcription factor NF-κB and is therefore suited for analysis on the translational level. However, small interfering RNAs are known to act on the post-transcriptional level. To evaluate their regulatory mechanisms in more detail, real-time quantitative PCRs (RT-qPCR) were carried out.

Cell lines were transfected with different regulatory miRNAs/siRNAs as well as reporter plasmid, to ensure identical conditions between all experimental methods. Subsequent real-time PCR was performed using a set of different primers, comprising two alternative splicing variants of p65 (RelA1, RelA2), miR-375 and the house-keeping gene RNU48. Table 3.2 is a summary of results for CCL227, depicting the measured crossing-points (CT), correlation coefficients, differences between CTs of samples upon introduction of foreign non-coding RNA (ΔCT) and the relative expression ratios obtained using the mathematical model developed by Pfaffl (Ratio).

When aiming to quantify p65, it is apparent that discrepancies between samples transfected with different types of miRNAs/siRNAs are not pronounced enough to allow for significant conclusions. Changes in ΔCT values show similar magnitudes as their corresponding standard deviations determined by intra-assay variation (n=4). p65-siR, which acts as down-regulator of RelA should in theory exhibit a negative ΔCT. In fact, measurements show the contradictory with corresponding to a slight upregulation of NF-κB expression, thus opposing results derived by other methods. miR-375, which is believed to act as an stimulator, even exhibits a slightly negative ΔCT, indicating that in the untreated parental cell line more mRNA specific for NF-κB is present. The largest deviation upon miRNA introduction is exhibited by miR-125b, showing a 2-fold change in cDNA levels and therefore upregulation of

NF-κB.

In order to validate efficient and successful transfection of miRNAs, primers complementary to miR-375 were used on cells transfected with the very same miRNA. A change in number of cycles by nearly 50% and a calculated fold change of approximately 7400, convincingly demonstrates successful introduction of foreign non-coding RNA.

Table 3.2: Overview results from RT-qPCR analysis for cell line CCL227. Depicted are the primers used (RelA1, RelA2, miR-375), the type of non-coding RNA transfected (neg.control, p65-siR, miR-375, miR-125b), the measured cycle number (CT), standard deviation (STD) and corresponding coefficient of variation (CV), as well as the calculated change in cycle number upon comparison to the negative control. The last column indicates the overall expressional fold change, derived by using the Pfafffl algorithm and RNU48 as reference gene. Data shown is the summary of several independently performed experiments.

	transfected miR/siR	CT [cycles]	STD [cycles]	CV [%]	ΔCT	Ratio
RelA1	control	31.18	0.70	2.25	-	-
	p65	30.51	1.19	3.90	0.66	0.56
	miR-375	32.13	1.49	4.64	-0.31	0.85
	miR-125b	29.98	0.86	2.87	1.84	1.99
RelA2	control	32.56	1.24	3.81	-	-
	p65	31.45	1.51	4.80	1.11	0.73
miR-375	control	33.45	0.37	1.11	-	-
	miR-375	17.16	0.09	0.52	16.29	7391.48

3.7 Viability assay after transfection of NF-κB modulating siRNA

Results from the luminescent assays suggest that p65-siR is able to efficiently suppress NF-κB. Based on this, it was examined whether this modulation is sufficient to restore susceptibility of resistant phenotype cell lines to 5-FU.

To evaluate cell viability upon exposure to 5-FU, MTT assays were carried out.

As seen in table 3.3, samples transfected with p65-siR show a lower IC50 value than the corresponding negative control, hinting at a decreasing ability to survive in presence of cytostatic agent (LR + p65-siR; IR + p65-siR). The low-resistance phenotype shows a slight but consistent viability reduction, displaying the therapeutic potential small regulatory RNA acting on inflammatory pathways possess (figure 3.10, dark red). When inspecting the nonlinear regression curve fit of the intermediate resistance clone (IR + p56-siR, figure 3.10, dark green), it is evident that the cells show a profoundly lower extinction at low concentrations of 5-FU. This can be explained by varying cell counts before adding the cytostatic agent. During transfection procedures, the viability of cells can be reduced. This is to be avoided, because to ensure reliable results when comparing different setups, a constant cell count is a premise. Respective effect was sought to be compensated by increasing the amount of seeded cells per well when working with transfected cells (see 2.4 for further information). As seen for the low-resistance phenotype (LR + p65-siR), respective approach can successfully compensate cell count discrepancies. This allows for reliable comparison of IC50 values, which tend to be lower for the transfected sample (table 3.3). In the case of IR + p65-siR, in which the number of seeded cells differ profoundly from its untransfected equivalent, over-interpretation of results is not advised. It must be mentioned, that further control probes must be added in order to fully differentiate between the impact of the transfection procedure itself and the effect of NF-κB inhibition on cell viability.

The 95% confidence interval of the calculated IC50s depicts a wide spread, indicating high variability amongst replicas. Lastly, the coefficient of determination (R^2) describes the relation between data and model and how well the model can describe the measured values. An R^2 of 1 designates perfect correlation. The correlation obtained in this experiment varies between 0.96 and 0.98, which is considered a good fit.

Table 3.3: 50% inhibitory concentrations (IC50) of low resistance and intermediate resistance phenotypes transfected with negative control siRNA (LR; IR) or p65-siRNA (LR + p65-siR; IR + p65-siR). Data are the mean±standard deviation. Dose-response curve were derived from a MTT assay.

	LR	LR + p65-siR	IR	IR + p65-siR
IC50	83.31± 0.1	47.31± 0.07	731.40± 0.08	249.12± 0.13
95% confidence interval (IC50)	50.37 - 137.8	34.47 - 64.45	495.2 - 1080	131.1 - 473.0
R^2	0.96	0.98	0.98	0.98

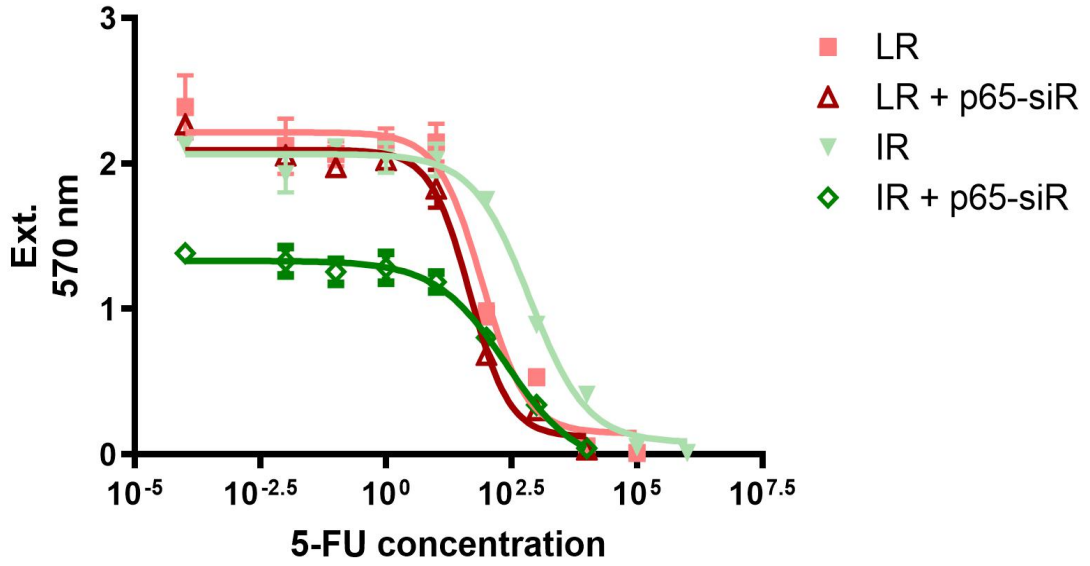

Figure 3.10: Dose response curves of low resistance (LR) and intermediate resistance (IR) phenotype upon transfection of p65-siRNA (LR + p65-siR; IR + p65-siR). Curves follow the familiar symmetrical sigmoidal shape. IC50 values were obtained following fit to model. The data represent mean SD (n = 3).

Discussion

Activation of the NF-κB signaling pathway in cancer tissue can be easily linked to tumor progression and development of resistances against chemotherapeutic agents. Previous work has shown, that upon examining progressive stages of resistance to 5-FU, unique genomic expression patterns can be observed [6]. Furthermore, abnormal expression of miRNAs, which are known to act as post-transcriptional regulators, are very common in malignant tissue [36]. This led to the hypothesis, that altered miRNA expression in cell lines insensitive to 5-FU might play an important role in the conferment of resistances. Preliminary experiments in the course of this study proved, that a colon carcinoma cell model showing resistance to 5-FU developed profound discrepancy in expression levels of several miRNAs.

Using a colonic carcinoma model system with multistage resistance to the widely used chemotherapeutic agent 5-FU enabled us to study the impact of a selected set of miRNAs suspected to have an impact on NF-κB signaling.

Independent on the degree of resistance NF-κB was shown to be highly activated in an *in vitro* multistage 5-FU resistant colonic carcinoma model, as indicated by the elevated expression of phospho-p65. Underlining this observation was the complete absence of phospho-p65 in the native chemosensitive cell lines [12]. Similar thereof, we found evidence of minor NF-κB activation in our chemosensitive naïve cell line CCL228. The lymph node metastasis CCL227 delivered a more controversial picture due to the fact, that measurements showcased high levels of NF-κB, as well as activa-

tion comparable to CCL228. This internal deviation could derive from slightly varying culture conditions promoting cellular stress responses subsequently triggering an inflammatory cell response. Low-resistance and intermediate-resistance phenotypes were found to highly express NF-κB, going in accordance with previous studies. The high-resistance cell line, however, only shows minor levels of the transcription factor. This unexpected finding might have different origins. It is established, that the initial acquirement of resistance involves heavy genomic alteration, indicating the challenges cells have to tackle. Once tolerant to chemotherapeutics, the conversion to higher resistance stages is less demanding [6]. Our result suggests, that pro-inflammatory signaling might be of special importance in the complex initial transition steps, whilst later it is rendered obsolete. This furthermore potentially hints at an unknown mechanism involved in formation of highly resistant phenotypes. Additionally, the methodological approach taken in this study substantially differed from other studies. Körber et al., for instance, used Western Blotting of whole cell lysates, allowing them detection of the whole NF-κB entity present in the cell. Our reporter system was located in the cytoplasm, due to the plasmid's inability of translocation into the nucleus. Thereby, we may have captured the spatial distribution known to happen upon NF-κB activation, in which phosphorylated NF-κB units migrate into the nucleus [74]. Our finding would indicate, that high-resistance phenotypes shuttle NF-κB much more efficiently than the other resistant subclones.

Stimulation of the NF-κB signaling pathway in an *in vitro* setup using cytokines is a common method during the study of inflammatory cell responses. Cytokines of choice are either recombinant TNFα, IL-1α or IL-1β in the micromolar concentration range [58, 75]. The kinetic study carried out in the course of this work using IL-1α comprised concentrations from the picomolar range up to 100 ng/mL. Although the highest concentration was chosen significantly higher than suggested

by literature (average concentrations ranging between 5 ng/mL - 10 ng/mL), no significant upregulation could be observed. Using rat glioma cells, Moynagh et al. could show, that stimulation using IL-1α is possible, but ten times less potent than stimulation with IL-1β [59]. This suggest differences in responses to IL-1 family members according to tissue type or organism and could explain the minor NF-κB activation we observed.

Aside from measuring base NF-κB activation in each cell line or trying to trigger an inflammatory response, our main goal was the alteration of transcription factor levels using RNA interference (RNAi). Firstly, transfection of siRNA compatible to the p65 unit of NF-κB (p65-siR) was carried out. siRNAs are known to work as post-transcriptional regulators through target mRNA degradation or inhibition of translation [76]. Going in accordance with theoretical knowledge, transfection of p65-siR in our study was able to significantly lower endogenous NF-κB levels independent on the degree of resistance. Variations in transfected amounts of p65-siR revealed, that concentrations five times lower than advised by the assay manufacturer diminish protein levels equally potent. This result is a strong affirmation of the potency of siRNA to act as regulatory element. qPCR experiments conducted showed, that the transcriptom remains unaltered upon siRNA introduction, which suggests p65-siR acts through inhibition of translation. Viability assays were carried out to test whether NF-κB inhibition through p65-siRNA is sufficient to alter response of chemoresistant cells to 5-FU. Low-resistance, as well as intermediate-resistance phenotypes showed an increase in susceptibility to 5-FU upon introduction of p65-siR. Although methodological inconsistencies require further replicates we have shown, that NF-κB activation may be an important resistance enhancing mechanism. Furthermore, alteration of NF-κB signaling *via* non-coding RNA appears to be a promising non-toxic way of coping with chemotherapeutic resistances. In order to validate our hypothesis, that miRNA highly abundant in cell lines in-

sensitive to 5-FU are involved in NF-κB activation, miR-125b and miR-375 were selected for transfection experiments. miR-125b was reported to constitutively activate NF-κB in diffuse large B-cell lymphomas by targeting its negative regulator tumor necrosis factor alpha-induced protein 3 (TNFAIP3) [47]. Going in accordance with this, our miRNA screen showed elevated levels of miR-125b in cell lines overexpressing NF-κB. Transfection of miR-mimetics however, did not alter protein levels significantly in either direction. This effect was not related to over-stimulation, as confirmed by the kinetic experiments carried out. Analysis on the transcript level revealed stimulating potencies by slightly elevating mRNA levels. The lack of major NF-κB activation could lie in the indirect modulation *via* TNFAIP3, leading to less pronounced results.

The second miRNA suspected to possess NF-κB stimulating potency delivers a picture controversial to common knowledge. Whilst our screen identified miR-375 as a potential NF-κB activator, another high-througput screening study reported its strong suppressing potencies [61]. Disagreements concerning screening assays may derive from the use of different cell lines, as Olarerin-George et al. used HEK293 cells and miRNA expression is known to be highly tissue specific [36]. Regardless, transfection of miR-375 in our experiments did result in up to 40% reduction of reporter activity in several cell lines. Also mRNA levels were slightly decreased, as indicated by negative cycle numbers in RT-qPCR experiments. However, miR-375 was not only able to act as suppressor, also elevation of NF-κB levels oculd be observed in the luminescent assay. To identify the source of this contradiction, further experiments or complementary methods may be necessary.

The second hypothesis postulated studied capablities of potential tumor suppressor miRNAs for which transfection including miR-141 were carried out.miR-141 is part of the miR-200 family and aberrantly expressed not only in colorectal cancer (CRC), but many malignant tumors. It is known to play a role in cellular pro-

cesses commonly dysfunctional in cancer, such as epithelial-mesenchymal transition (EMT), proliferation, and migration [77]. The miRNA array performed by us classified miR-141 as potential tumor suppressor miRNA due to its elevated expression in the primary adenocarcinoma line CCL228 compared to other cell lines. Transfection experiments revealed the moderate potency of miR-141 to inhibit NF-κB signaling. Without reaching a significant reduction of protein levels, a clear trend is visible. Other studies working with ovarian tumor models however noted, that this miRNA exhibited higher abundances in chemotherapy resistant phenotypes [56]. These claims contradictory to our assay may hint at the histological-dependency of miR-141 expression. Recently, it was found to play a dual role as either oncogene or tumor-suppressor gene, depending on the context. Intriguingly, the function of miR-141 is very inconsistent and seems to not only be tissue dependent, as it has been reported to promote opposing cellular mechanisms within the same tissue type. As an example thereof serves CRC, where overexpression of miR-141 was reported to promote cell proliferation but is also able to limit migration and invasion of cancer cells [78, 79]. Also its involvement in NF-κB signaling is a disputbale topic. In an ovarian cancer model, miR-141 was identified to activate NF-κB by targeting an IKKβ inhibitor. Respective study even showed the subsequent enhancement of resistance to cisplatin based treatments, which directly links overexpression of a miRNA to chemoresistance [56]. However, research to miR-141 in prostate cancer tissue revealed, that it inhibits NF-κB signaling by directly targeting tumor necrosis factor receptor-associated factor 5 (TRAF5) and 6 (TRAF6). Further research on putative miR-141 targets in different model system is needed to clarify its functionality in the context of tumor progression.

Summarizing the results obtained by all experiments working with miRNA, it must be noted that the approaches chosen in this study have specific limitations. Firstly, the mode of miRNA selection can be criticized as unspecific and susceptible to mis-

interpretations, for it assumes the differential expression of several miRNA is mainly involved in the divergence concerning NF-κB activation in our multistage resistance model. This assumption may be viewed as too simplistic, as miRNA are known to work in complex unison with other cellular mechanisms. The effect of introducing a single miRNA alone is logical to be limited, as observable in this study.
Additionally, we must take into account technical difficulties faced during the practical aspects of this thesis. The coefficient of variation throughout transfection experiments can be regarded as rather large. This hints at an unoptimized assay or differing culture conditions, which can be accounted to the limited time frame faced during this work. Especially the transfection of resistant subtypes was found to be difficult, probably due to active efflux mechanisms cells have developed during resistance acquirement. Although quantitative RT-PCR is regarded as a stable and robust method, many replicas were needed to allow for a confident interpretation. Subsequent to the practical aspect of this study, it was noted that there were technical issues with the temperature sensor built into the thermocycler used during cDNA amplification. Therefore it must be mentioned, that all qPCR results should be interpreted with care.

In conclusion, our results showed that NF-κB is differentially expressed in cell lines sensitive and insensitive to the chemotherapeutic agent 5-FU. Interestingly, the high-resistance phenotype exhibited similar expression patterns to the naïve cell line, suggesting different cellular mechanisms involved in conferring total resistance to a drug.
Reliable inhibition of NF-κB signaling through RNA interference was only possible using siRNA targeted at the p65 subunit of the protein complex. Preliminary viability assays uncovered the potential of p65-siR to even restore susceptibility of chemoresistant phenotypes to 5-FU. miR-125b and miR-375, which were sought to

be indirectly linked to resistance conferment *via* NF-κB stimulation, were unable to elevate expression levels in this *in vitro* model. The proposed tumor suppressor miRNA, miR-141, could not be shown to prohibit inflammatory signaling.

By inhibiting inflammatory signaling pathways, it is sought to limit development of resistances to chemotherapeutic agents. Our data sheds light on the potential of lowering malignant NF-κB levels using RNA interference techniques. It furthermore emphasizes the complex role miRNAs play in cellular mechanisms. Examination of individual deregulated miRNAs does not suffice and hardly explains the observed phenotypic behavior.

To further deepen the insight on miRNAs as therapeutics, their target proteins must be thoroughly described. Also anti-miRNAs and their effect on deregulated cellular signaling is yet to be described in relevant model systems. As proof of concept, it would be highly interesting aiming to change the phenotype of a cell line by only altering its miRNA expression profile. Although up to today miRNA research remains a field with many open questions, the potential of RNA interference as new therapeutic approach is indisputable.

References

[1] Jeffrey A Meyerhardt and Robert J Mayer. Systemic therapy for colorectal cancer. *New England Journal of Medicine*, 352(5):476–487, 2005.

[2] Ning Zhang, Ying Yin, Sheng-Jie Xu, and Wei-Shan Chen. 5-fluorouracil: mechanisms of resistance and reversal strategies. *Molecules*, 13(8):1551–1569, 2008.

[3] Richard M Goldberg, Daniel J Sargent, Roscoe F Morton, Charles S Fuchs, Ramesh K Ramanathan, Stephen K Williamson, Brian P Findlay, Henry C Pitot, and Steven R Alberts. A randomized controlled trial of fluorouracil plus leucovorin, irinotecan, and oxaliplatin combinations in patients with previously untreated metastatic colorectal cancer. *Journal of Clinical Oncology*, 22(1):23–30, 2004.

[4] Robert M Mader, Markus Müller, and Günther G Steger. Resistance to 5-fluorouracil. *General Pharmacology: The Vascular System*, 31(5):661–666, 1998.

[5] Michael M Gottesman. Mechanisms of cancer drug resistance. *Annual review of medicine*, 53(1):615–627, 2002.

[6] Wolfgang M Schmidt, Maria Kalipciyan, Eva Dornstauder, Blanka Rizovski, Guenther G Steger, Roland Sedivy, Manfred W Mueller, and Robert M Mader. Dissecting progressive stages of 5-fluorouracil resistance in vitro using rna expression profiling. *International journal of cancer*, 112(2):200–212, 2004.

[7] Karin E. de Visser and Jos Jonkers. Towards understanding the role of cancer-associated inflammation in chemoresistance. *Current Pharmaceutical Design*, 15(16):1844–1853, 2009.

[8] Lisa M Coussens and Zena Werb. Inflammation and cancer. *Nature*, 420(6917):860, 2002.

[9] Michael Karin and Tony Hunter. Transcriptional control by protein phosphorylation: signal transmission from the cell surface to the nucleus. *Current Biology*, 5(7):747–757, 1995.

[10] Xinglong Qu, Ying Tang, and Shucheng Hua. Immunological approaches towards cancer and inflammation: A cross talk. *Frontiers in Immunology*, 9:563, 2018.

[11] Haitian Lu, Weiming Ouyang, and Chuanshu Huang. Inflammation, a key event in cancer development. *Molecular Cancer Research*, 4(4):221–233, 2006.

[12] Maria Isabel Koerber, Anna Staribacher, INA Ratzenböck, Guenther Steger, and Robert M Mader. Nfκb-associated pathways in progression of chemoresistance to 5-fluorouracil in an in vitro model of colonic carcinoma. *Anticancer research*, 36(4):1631–1639, 2016.

[13] Wei Li, Dongfeng Tan, Maryam J Zenali, and Robert E Brown. Constitutive activation of nuclear factor-kappa b (nf-kb) signaling pathway in fibrolamellar hepatocellular carcinoma. *International journal of clinical and experimental pathology*, 3(3):238, 2010.

[14] Soly Wang, Zhanjie Liu, Lunshan Wang, and Xiaoren Zhang. Nf-κb signaling pathway, inflammation and colorectal cancer. *Cellular & molecular immunology*, 6(5):327, 2009.

[15] Eli Pikarsky, Rinnat M Porat, Ilan Stein, Rinat Abramovitch, Sharon Amit, Shafika Kasem, Elena Gutkovich-Pyest, Simcha Urieli-Shoval, Eithan Galun, and Yinon Ben-Neriah. Nf-κb functions as a tumour promoter in inflammation-associated cancer. *Nature*, 431(7007):461, 2004.

[16] D Scott Lind, Steven N Hochwald, John Malaty, Stelio Rekkas, Paul Hebig, Girish Mishra, Lyle L Moldawer, Edward M Copeland III, and Sally MacKay. Nuclear factor-κb is upregulated in colorectal cancer. *Surgery*, 130(2):363–369, 2001.

[17] Hong Jin Kim, N Hawke, and Albert S Baldwin. Nf-κb and ikk as therapeutic targets in cancer. *Cell death and differentiation*, 13(5):738, 2006.

[18] Yumi Yamamoto and Richard B Gaynor. Therapeutic potential of inhibition of the nf-κb pathway in the treatment of inflammation and cancer. *The Journal of clinical investigation*, 107(2):135–142, 2001.

[19] Sankar Ghosh and Michael Karin. Missing pieces in the nf-κb puzzle. *cell*, 109(2):S81–S96, 2002.

[20] Keith Brown, Susan Gerstberger, Louise Carlson, Guido Franzoso, and Ulrich Siebenlist. Control of i kappa b-alpha proteolysis by site-specific, signal-induced phosphorylation. *Science*, 267(5203):1485–1488, 1995.

[21] Patrick Viatour, Marie-Paule Merville, Vincent Bours, and Alain Chariot. Phosphorylation of nf-κb and iκb proteins: implications in cancer and inflammation. *Trends in biochemical sciences*, 30(1):43–52, 2005.

[22] Thomas A Halsey, Longlong Yang, John R Walker, John B Hogenesch, and Russell S Thomas. A functional map of nfκb signaling identifies novel modulators and multiple system controls. *Genome biology*, 8(6):R104, 2007.

[23] Cun-Yu Wang, James C Cusack Jr, Rong Liu, and Albert S Baldwin Jr. Control of inducible chemoresistance: enhanced anti-tumor therapy through increased apoptosis by inhibition of nf-κb. *Nature medicine*, 5(4):412, 1999.

[24] Dung-Fang Lee and Mien-Chie Hung. Advances in targeting ikk and ikk-related kinases for cancer therapy. *Clinical Cancer Research*, 14(18):5656–5662, 2008.

[25] Alex Yemelyanov, A Gasparian, P Lindholm, L Dang, JW Pierce, F Kisseljov, A Karseladze, and Irina Budunova. Effects of ikk inhibitor ps1145 on nf-κb function, proliferation, apoptosis and invasion activity in prostate carcinoma cells. *Oncogene*, 25(3):387, 2006.

[26] Paul Richardson, Teru Hideshima, Constantine Mitsiades, and Kenneth Anderson. Proteasome inhibition in hematologic malignancies. *Annals of Medicine*, 36(4):304–314, 2004. PMID: 15224657.

[27] Dong Yin, Hong Zhou, Takashi Kumagai, Gentao Liu, John M Ong, Keith L Black, and H Phillip Koeffler. Proteasome inhibitor ps-341 causes cell growth arrest and apoptosis in human glioblastoma multiforme (gbm). *Oncogene*, 24(3):344, 2005.

[28] Alexander V Gasparian, Olga A Guryanova, Dmitry V Chebotaev, Alexander A Shishkin, Alexander Y Yemelyanov, and Irina V Budunova. Targeting transcription factor nfκb: comparative analysis of proteasome and ikk inhibitors. *Cell Cycle*, 8(10):1559–1566, 2009.

[29] Philippe Moreau, Paul G Richardson, Michele Cavo, Robert Z Orlowski, Jesús F San Miguel, Antonio Palumbo, and Jean-Luc Harousseau. Proteasome inhibitors in multiple myeloma: 10 years later. *Blood*, 120(5):947–959, 2012.

[30] Iris Lavon, Iris Goldberg, Sharon Amit, Limor Landsman, Steffen Jung, Ben-Zion Tsuberi, Iris Barshack, Juri Kopolovic, Eitan Galun, Hermann Bujard,

et al. High susceptibility to bacterial infection, but no liver dysfunction, in mice compromised for hepatocyte nf-κb activation. *Nature medicine*, 6(5):573, 2000.

[31] David P Bartel. Micrornas: genomics, biogenesis, mechanism, and function. *cell*, 116(2):281–297, 2004.

[32] Kaladhar B Reddy. Microrna (mirna) in cancer. *Cancer cell international*, 15(1):38, 2015.

[33] Ramiro Garzon, George A Calin, and Carlo M Croce. Micrornas in cancer. *Annual review of medicine*, 60:167–179, 2009.

[34] Daehyun Baek, Judit Villén, Chanseok Shin, Fernando D Camargo, Steven P Gygi, and David P Bartel. The impact of micrornas on protein output. *Nature*, 455(7209):64, 2008.

[35] Josie Hayes, Pier Paolo Peruzzi, and Sean Lawler. Micrornas in cancer: biomarkers, functions and therapy. *Trends in molecular medicine*, 20(8):460–469, 2014.

[36] JM Cummins and VE Velculescu. Implications of micro-rna profiling for cancer diagnosis. *Oncogene*, 25(46):6220, 2006.

[37] Yong Peng and Carlo M Croce. The role of micrornas in human cancer. *Signal transduction and targeted therapy*, 1:15004, 2016.

[38] Nina Raver-Shapira, Efi Marciano, Eti Meiri, Yael Spector, Nitzan Rosenfeld, Neta Moskovits, Zvi Bentwich, and Moshe Oren. Transcriptional activation of mir-34a contributes to p53-mediated apoptosis. *Molecular cell*, 26(5):731–743, 2007.

[39] Douglas Hanahan and Robert A Weinberg. Hallmarks of cancer: the next generation. *cell*, 144(5):646–674, 2011.

[40] George A Calin and Carlo M Croce. Microrna signatures in human cancers. *Nature reviews cancer*, 6(11):857, 2006.

[41] Andrea L Kasinski and Frank J Slack. Micrornas en route to the clinic: progress in validating and targeting micrornas for cancer therapy. *Nature Reviews Cancer*, 11(12):849, 2011.

[42] Chiranjib Chakraborty, Ashish Ranjan Sharma, Garima Sharma, C George Priya Doss, and Sang-Soo Lee. Therapeutic mirna and sirna: moving from bench to clinic as next generation medicine. *Molecular Therapy-Nucleic Acids*, 8:132–143, 2017.

[43] Rajesha Rupaimoole and Frank J Slack. Microrna therapeutics: towards a new era for the management of cancer and other diseases. *Nature reviews Drug discovery*, 16(3):203, 2017.

[44] Xiaodong Ma, Lindsey E Becker Buscaglia, Juanita R Barker, and Yong Li. Micrornas in nf-κb signaling. *Journal of molecular cell biology*, 3(3):159–166, 2011.

[45] D Bhaumik, GK Scott, S Schokrpur, CK Patil, J Campisi, and CC Benz. Expression of microrna-146 suppresses nf-κb activity with reduction of metastatic potential in breast cancer cells. *Oncogene*, 27(42):5643, 2008.

[46] Shawn M Egan, Ellen Karasik, Leigh Ellis, and Sandra O Gollnick. mir-30e* is overexpressed in prostate cancer and promotes nf-κb-mediated proliferation and tumor growth. *Oncotarget*, 8(40):67626, 2017.

[47] Sang-Woo Kim, Kumaraguruparan Ramasamy, Hakim Bouamar, An-Ping Lin, Daifeng Jiang, and Ricardo CT Aguiar. Micrornas mir-125a and mir-125b constitutively activate the nf-κb pathway by targeting the tumor necrosis factor alpha-induced protein 3 (tnfaip3, a20). *Proceedings of the National Academy of Sciences*, 109(20):7865–7870, 2012.

[48] Yeqian Feng, Shenghua Zhou, Guiyuan Li, Chunhong Hu, Wen Zou, Haixia Zhang, and Lili Sun. Nuclear factor-κb–dependent microrna-130a upregulation promotes cervical cancer cell growth by targeting phosphatase and tensin homolog. *Archives of biochemistry and biophysics*, 598:57–65, 2016.

[49] Tongsen Zheng, Jiabei Wang, Xi Chen, and Lianxin Liu. Role of microrna in anticancer drug resistance. *International journal of cancer*, 126(1):2–10, 2010.

[50] Ci Zhao, Qi Zhao, Chunhui Zhang, Guangyu Wang, Yuanfei Yao, Xiaoyi Huang, Fei Zhan, Yuanyuan Zhu, Jiaqi Shi, Jianan Chen, et al. mir-15b-5p resensitizes colon cancer cells to 5-fluorouracil by promoting apoptosis via the nf-κb/xiap axis. *Scientific reports*, 7(1):4194, 2017.

[51] Graham McClorey and Matthew J Wood. An overview of the clinical application of antisense oligonucleotides for rna-targeting therapies. *Current opinion in pharmacology*, 24:52–58, 2015.

[52] Li Huang, Fang Li, Pengbo Deng, and Chengping Hu. Microrna-223 promotes tumor progression in lung cancer a549 cells via activation of the nf-κb signaling pathway. *Oncology Research Featuring Preclinical and Clinical Cancer Therapeutics*, 24(6):405–413, 2016.

[53] Chuan He Yang, Junming Yue, Michelle Sims, and Lawrence M Pfeffer. The curcumin analog ef24 targets nf-κb and mirna-21, and has potent anticancer activity in vitro and in vivo. *PloS one*, 8(8):e71130, 2013.

[54] Yi-Jing Tao, Yong-ju Li, Wen Zheng, Juan-juan Zhao, Meng-meng Guo, Ya Zhou, Na-lin Qin, Jing Zheng, and Lin Xu. Antisense oligonucleotides against microrna-21 reduced the proliferation and migration of human colon carcinoma cells. *Cancer cell international*, 15(1):77, 2015.

[55] Su Xiao, Yu-Chi Chen, Michael J Betenbaugh, Scott E Martin, and Joseph Shiloach. Mirna mimic screen for improved expression of functional neurotensin receptor from hek 293 cells. *Biotechnology and bioengineering*, 112(8):1632–1643, 2015.

[56] MTM Van Jaarsveld, Jozien Helleman, AWM Boersma, PF Van Kuijk, WF Van Ijcken, Evelyn Despierre, Ignace Vergote, RHJ Mathijssen, EMJJ Berns, Jaap Verweij, et al. mir-141 regulates keap1 and modulates cisplatin sensitivity in ovarian cancer cells. *Oncogene*, 32(36):4284, 2013.

[57] Maria Angelica Cortez, David Valdecanas, Xiaochun Zhang, Yanai Zhan, Vikas Bhardwaj, George A Calin, Ritsuko Komaki, Dipak K Giri, Caio C Quini, Tatiana Wolfe, et al. Therapeutic delivery of mir-200c enhances radiosensitivity in lung cancer. *Molecular Therapy*, 22(8):1494–1503, 2014.

[58] A A Beg, T S Finco, P V Nantermet, and A S Baldwin. Tumor necrosis factor and interleukin-1 lead to phosphorylation and loss of i kappa b alpha: a mechanism for nf-kappa b activation. *Molecular and Cellular Biology*, 13(6):3301–3310, 1993.

[59] Paul N Moynagh, D Clive Williams, and Luke AJ O'Neill. Interleukin-1 activates transcription factor nfκ b in glial cells. *Biochemical Journal*, 294(2):343–347, 1993.

[60] Y Yang and JK Wang. The functional analysis of micrornas involved in nf-κb signaling. *Eur Rev Med Pharmacol Sci*, 20(9):1764–1774, 2016.

[61] Anthony O Olarerin-George, Lauren Anton, Yih-Chii Hwang, Michal A Elovitz, and John B Hogenesch. A functional genomics screen for microrna regulators of nf-kappab signaling. *BMC biology*, 11(1):19, 2013.

[62] Shuai Huang, Qingde Wa, Jincheng Pan, Xinsheng Peng, Dong Ren, Yan Huang, Xiao Chen, and Yubo Tang. Downregulation of mir-141-3p promotes bone metastasis via activating nf-κb signaling in prostate cancer. *Journal of Experimental & Clinical Cancer Research*, 36(1):173, 2017.

[63] Silvia Antolín, Lourdes Calvo, Moisés Blanco-Calvo, María Paz Santiago, María José Lorenzo-Patiño, Mar Haz-Conde, Isabel Santamarina, Angélica Figueroa, Luis Miguel Antón-Aparicio, and Manuel Valladares-Ayerbes. Circulating mir-200c and mir-141 and outcomes in patients with breast cancer. *BMC cancer*, 15(1):297, 2015.

[64] Reiner Westermeier and Rita Marouga. Protein detection methods in proteomics research. *Bioscience Reports*, 25(1-2):19–32, 2005.

[65] Jacob O'Brien, Heyam Hayder, Yara Zayed, and Chun Peng. Overview of microrna biogenesis, mechanisms of actions, and circulation. *Frontiers in endocrinology*, 9:402, 2018.

[66] Willard M Freeman, Stephen J Walker, and Kent E Vrana. Quantitative rt-pcr: pitfalls and potential. *Biotechniques*, 26(1):112–125, 1999.

[67] Tom B Morrison, Janis J Weis, and Carl T Wittwer. Quantification of low-copy transcripts by continuous sybr green i monitoring during amplification. *Biotechniques*, 24(6):954–8, 1998.

[68] Michael W Pfaffl. A new mathematical model for relative quantification in real-time rt–pcr. *Nucleic acids research*, 29(9):e45–e45, 2001.

[69] Tim Mosmann. Rapid colorimetric assay for cellular growth and survival: application to proliferation and cytotoxicity assays. *Journal of immunological methods*, 65(1-2):55–63, 1983.

[70] Michael V Berridge and An S Tan. Characterization of the cellular reduction of 3-(4, 5-dimethylthiazol-2-yl)-2, 5-diphenyltetrazolium bromide (mtt): subcellular localization, substrate dependence, and involvement of mitochondrial electron transport in mtt reduction. *Archives of biochemistry and biophysics*, 303(2):474–482, 1993.

[71] Michael V Berridge, Patries M Herst, and An S Tan. Tetrazolium dyes as tools in cell biology: new insights into their cellular reduction. *Biotechnology annual review*, 11:127–152, 2005.

[72] Denese C Marks, Larissa Belov, Mary W Davey, Ross A Davey, and Antony D Kidman. The mtt cell viability assay for cytotoxicity testing in multidrug-resistant human leukemic cells. *Leukemia research*, 16(12):1165–1173, 1992.

[73] Jean M Sargent. The use of the mtt assay to study drug resistance in fresh tumour samples. In *Chemosensitivity Testing in Oncology*, pages 13–25. Springer, 2003.

[74] Orla Maguire, Christine Collins, Kieran O'Loughlin, Jeffrey Miecznikowski, and Hans Minderman. Quantifying nuclear p65 as a parameter for nf-κb activation: Correlation between imagestream cytometry, microscopy, and western blot. *Cytometry Part A*, 79(6):461–469, 2011.

[75] Gloria JF Ding, Paul A Fischer, Robert C Boltz, Jack A Schmidt, James J Colaianne, Albert Gough, Richard A Rubin, and Douglas K Miller. Characterization and quantitation of nf-κb nuclear translocation induced by interleukin-1 and

tumor necrosis factor-α development and use of a high capacity fluorescence cytometric system. *Journal of Biological Chemistry*, 273(44):28897–28905, 1998.

[76] Richard W Carthew and Erik J Sontheimer. Origins and mechanisms of mirnas and sirnas. *Cell*, 136(4):642–655, 2009.

[77] Yanping Gao, Bing Feng, Siqi Han, Kai Zhang, Jing Chen, Chen Li, Rui Wang, and Longbang Chen. The roles of microrna-141 in human cancers: from diagnosis to treatment. *Cellular Physiology and Biochemistry*, 38(2):427–448, 2016.

[78] Lei Ding, Li-Li Yu, Ning Han, and Bu-Tian Zhang. mir-141 promotes colon cancer cell proliferation by inhibiting map2k4. *Oncology letters*, 13(3):1665–1671, 2017.

[79] Minghua Hu, MicroGene Xia, Xiaobing Chen, Zihong Lin, Yajun Xu, Yuedong Ma, and Lei Su. Microrna-141 regulates smad interacting protein 1 (sip1) and inhibits migration and invasion of colorectal cancer cells. *Digestive diseases and sciences*, 55(8):2365–2372, 2010.